Article

Cell

A Conserved Bicycle Model for Circadian Clock Control of Membrane Excitability

Graphical Abstract

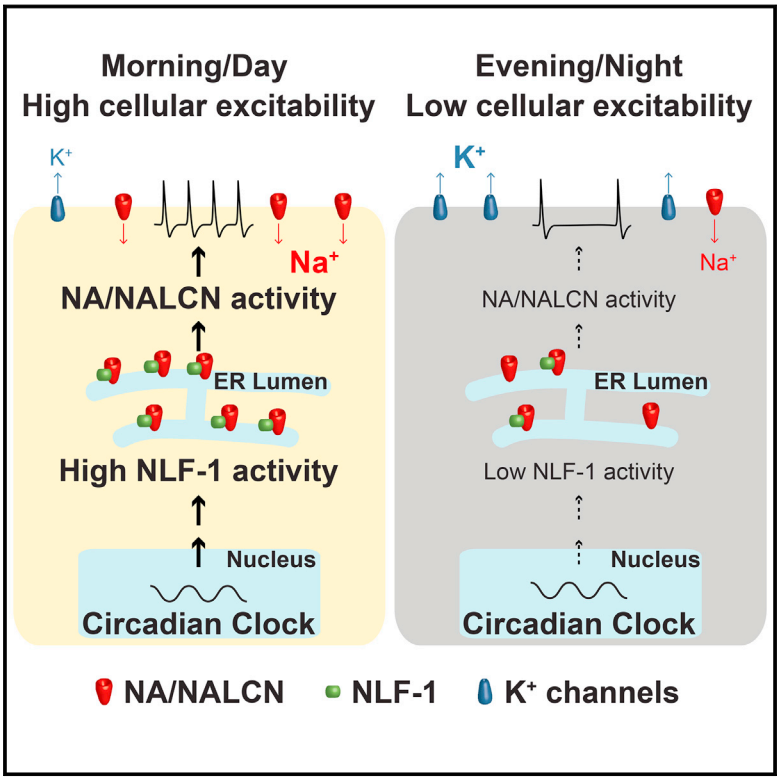

Highlights

- Rhythmic sodium leak conductance depolarizes *Drosophila* circadian pacemaker neurons
- NCA localization factor 1 links the molecular clock to sodium leak channel activity
- Antiphase cycles in resting K^+ and Na^+ conductances drive membrane potential rhythms
- This "bicycle" mechanism is conserved in master clock neurons between flies and mice

Authors

Matthieu Flourakis, Elzbieta Kula-Eversole, Alan L. Hutchison, ..., Casey O. Diekman, Indira M. Raman, Ravi Allada

Correspondence

r-allada@northwestern.edu

In Brief

Two distinctly timed sodium and potassium electrical drives collaborate to directly control membrane excitability and neuronal function in a circadian manner.

Flourakis et al., 2015, Cell *162*, 836–848
August 13, 2015
http://dx.doi.org/10.1016/j.cell.2015.07.036

CellPress

Cell

Article

A Conserved Bicycle Model for Circadian Clock Control of Membrane Excitability

Matthieu Flourakis,[1] Elzbieta Kula-Eversole,[1] Alan L. Hutchison,[2] Tae Hee Han,[1] Kimberly Aranda,[3] Devon L. Moose,[4] Kevin P. White,[5] Aaron R. Dinner,[2] Bridget C. Lear,[4] Dejian Ren,[3] Casey O. Diekman,[6] Indira M. Raman,[1] and Ravi Allada[1,*]

[1]Department of Neurobiology, Northwestern University, Evanston, IL 60208, USA

[2]Medical Scientist Training Program, James Franck Institute, Department of Chemistry, Institute for Biophysical Dynamics, University of Chicago, Chicago, IL 60637, USA

[3]Department of Biology, University of Pennsylvania, Philadelphia, PA 19104, USA

[4]Department of Biology, University of Iowa, Iowa City, IA 52242, USA

[5]Institute for Genomics and Systems Biology, University of Chicago, Chicago, IL 60637, USA

[6]Department of Mathematical Sciences, New Jersey Institute of Technology, Newark, NJ 07102, USA

*Correspondence: r-allada@northwestern.edu

http://dx.doi.org/10.1016/j.cell.2015.07.036

SUMMARY

Circadian clocks regulate membrane excitability in master pacemaker neurons to control daily rhythms of sleep and wake. Here, we find that two distinctly timed electrical drives collaborate to impose rhythmicity on *Drosophila* clock neurons. In the morning, a voltage-independent sodium conductance via the NA/NALCN ion channel depolarizes these neurons. This current is driven by the rhythmic expression of NCA localization factor-1, linking the molecular clock to ion channel function. In the evening, basal potassium currents peak to silence clock neurons. Remarkably, daily antiphase cycles of sodium and potassium currents also drive mouse clock neuron rhythms. Thus, we reveal an evolutionarily ancient strategy for the neural mechanisms that govern daily sleep and wake.

INTRODUCTION

Circadian clocks have evolved to align organismal biochemistry, physiology, and behavior to daily environmental oscillations. At the core of these clocks in all multicellular organisms are conserved transcriptional feedback loops (Allada and Chung, 2010; Hardin, 2011). In *Drosophila*, the bHLH-PAS transcription factor heterodimer CLOCK (CLK) and CYCLE (CYC) directly binds E boxes (CACGTG) in target promoters of the clock genes, *period* (*per*) and *timeless* (*tim*), and activates their transcription. PER and TIM proteins feed back to repress CLK/CYC activity. The temporal separation of transcriptional activation and repression and/or mRNA and protein oscillations, in some cases by many hours (Lee et al., 1998), results in robust daily oscillations of *per*, *tim*, and other rhythmic transcripts. These molecular clocks, in turn, control a broad range of cellular and physiological responses likely via the rhythmic transcription of clock output genes.

While molecular clocks are expressed in a variety of cell types, those in specific circadian clock neurons in the brain exhibit special properties. These so-called "master" circadian pacemakers, such as the mammalian suprachiasmatic nucleus (SCN) and the *Drosophila* lateral and dorsal neurons, drive robust 24 hr rhythms of sleep and wake behavior (Helfrich-Förster, 2005; Mohawk and Takahashi, 2011). Unlike generic clock cells, these clock neurons are interconnected via neural networks and, as a result, produce coherent and sustained free running molecular and behavioral rhythmicity under constant conditions (Flourakis and Allada, 2015; Guo et al., 2014; Peng et al., 2003; Seluzicki et al., 2014; Shafer et al., 2002; Yang and Sehgal, 2001; Yao and Shafer, 2014). Although the anatomical features of brain pacemaker networks are highly divergent between mammals and invertebrates such as *Drosophila*, their ability to control sleep and wake cycles uniformly depends on daily rhythms of membrane excitability (Cao and Nitabach, 2008; Colwell, 2011; de Jeu et al., 1998; Kuhlman and McMahon, 2004; Sheeba et al., 2008). However, the mechanistic links between the molecular clock and the machinery controlling cellular excitability are not well understood.

Using patch-clamp analysis of the *Drosophila* DN1p, we show for the first time that circadian clock control of membrane excitability operates via resting sodium leak conductance through the narrow abdomen (NA) channel, providing timed depolarizing drive to circadian pacemaker neurons. We demonstrate that the sodium leak rhythm depends on rhythmic expression of NCA localization factor 1, linking the molecular clock and membrane excitability. We reveal that both flies and mice, separated by hundreds of millions of years in evolution, utilize antiphase oscillations of sodium and potassium conductances to drive clock control of membrane potential. Thus, the conservation of clock mechanisms between invertebrates and vertebrates extends from core timing mechanisms to the control of membrane excitability in the master clock neurons governing sleep and wake.

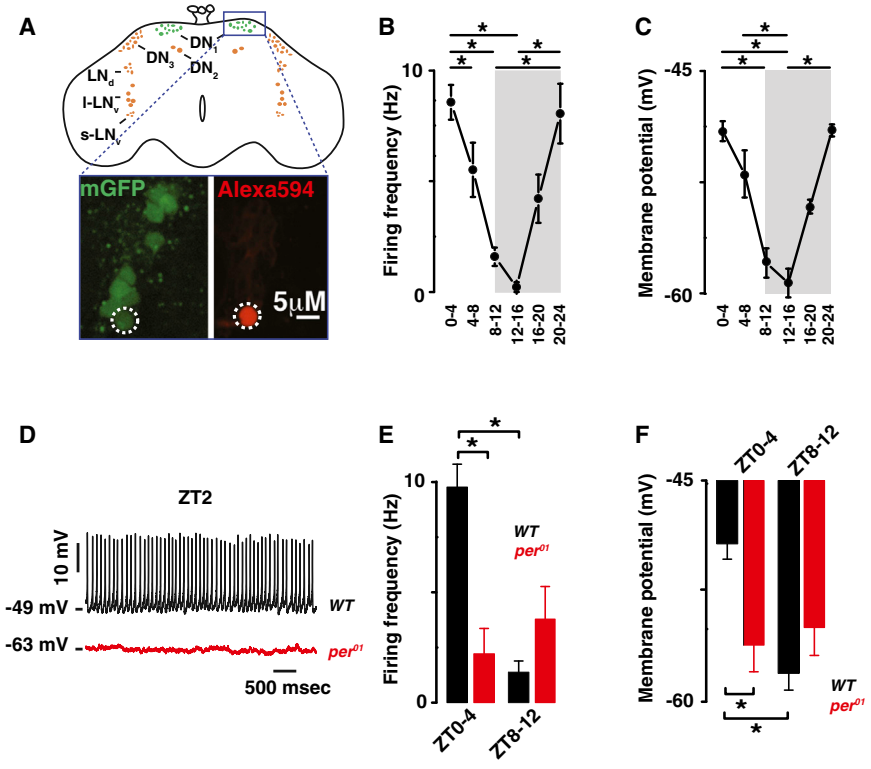

Figure 1. The Cellular Excitability of the *Drosophila* DN1p Circadian Pacemaker Neurons Is Clock Controlled

(A–C) (A) Schematic and image of the *Drosophila* brain indicating the location of the DN1ps and other clock neurons. Representative images of the GFP-expressing DN1ps in the intact *Drosophila* brain are shown below. The DN1ps were labeled by using the Clk4.1M-G4 driving the expression of U-CD8-GFP. Whole-cell access to GFP-labeled neurons was confirmed following diffusion of Alexa Fluor 594 biocytin included in intracellular recording solution. All recorded *WT* neurons are plotted against time of day (in 4 hr bins) to show daily rhythms of firing frequency (B) and membrane potential (C). Gray areas represent the dark phase of the LD cycle. Asterisks indicate statistical significance ($p < 0.05$) from a one-way ANOVA, Tukey's post hoc test.

(D–F) (D) Representative current-clamp recordings at Zeitgeber Time 2 (ZT2) showing that the per^{01} DN1p neurons (red) are hyperpolarized and silent compared to *WT* DN1p neurons (black). Histogram showing the decrease in firing frequency (E) and membrane potential (F) and lack of daily rhythm in per^{01} (red, 2.2 ± 1.1Hz, −56 ± 2 mV, n = 15 at ZT0–4 and 3.9 ± 1.5Hz, −55 ± 1.9 mV, n = 10 at ZT8–12, $p > 0.41$) when compared to *WT* (black) DN1p neurons. Results are expressed as mean ± SEM. Asterisks indicate statistical significance ($p < 0.05$) from t test performed in *WT* at ZT0–4 versus ZT8–12. See also Figures S1 and S2 and Tables S1 and S2.

RESULTS

Rhythmic Resting Potassium and Sodium Leak Currents Collaborate to Drive Clock-Controlled Excitability of the *Drosophila* Circadian Neurons

To elucidate the mechanistic basis of daily changes in membrane excitability in *Drosophila* clock neurons, we performed whole-cell patch-clamp electrophysiology on the posterior dorsal neurons 1 (DN1p) on explanted brains (Flourakis and Allada, 2015; Seluzicki et al., 2014). DN1p neurons harbor molecular circadian clocks, and under 12 hr light-12 hr dark (LD) conditions, they contribute to increases in locomotor activity in advance of lights-on (i.e., morning anticipation) and lights-off (i.e., evening anticipation) (Zhang et al., 2010a, 2010b). In addition to their established function in circadian behavior, the DN1p are an attractive target for patch-clamp analysis, as we can selectively label and identify DN1p neurons using the Clk4.1M-GAL4 driver in combination with UAS-CD8-GFP (Zhang et al., 2010a, 2010b) (Figure 1A). Furthermore, the DN1p neurons are easily accessible by electrode, as they are located near the brain surface (Flourakis and Allada, 2015; Seluzicki et al., 2014).

Using whole-cell patch-clamp analysis, a large daily variation in the firing frequency was detected (Figure 1B, $p < 0.05$, and Figure S1A). The wild-type (*WT*) DN1ps fire at ~10 Hz in the morning (Zeitgeber Time, ZT0–4) and are nearly silent in the evening (ZT8–12) (Table S1A). The firing frequency in cell-attached configuration was comparable to that observed in whole-cell mode (Figures S1B–S1D), suggesting that dialysis did not alter measurements of firing rates. The membrane potential also exhibited a temporal pattern: more depolarized in the morning than in the evening (Figure 1C, $p < 0.05$, and Table S1B). The neurons show daily rhythmic cellular excitability: more responsive to depolarizing currents in the morning than in the evening (Figure S1E and Table S2A). The input resistance had no significant diurnal rhythm (Figure S1F and Table S1C). The rhythms in firing frequency and membrane potential were not evident in the arrhythmic core clock mutant per^{01}, indicating that the canonical clock controls daily changes in intrinsic membrane properties. Compared to *WT*, the per^{01} neurons are hyperpolarized (Figure 1D) and show no rhythm in firing frequency (Figure 1E, $p = 0.41$), membrane potential (Figure 1F, $p = 0.66$), or cellular excitability (Figure S2A, $p > 0.41$). The per^{01} neurons also require more depolarizing current to fire at the same rates as *WT* (Figure S2B and Table S2B). Importantly, the high-amplitude daily rhythms in firing frequency observed in *WT* neurons exceed those previously described in another set of *Drosophila* circadian neurons (LNvs) and more closely approximate those described in mammalian SCN clock neurons (Cao and Nitabach, 2008; Colwell, 2011; Kuhlman and McMahon, 2006; Park and Griffith, 2006; Schaap et al., 2003; Sheeba et al., 2008), indicating that DN1p analysis will be useful to define the mechanisms for clock control of membrane excitability. Given the role of the DN1p in morning and evening behaviors (Zhang et al., 2010a, 2010b), these activity measurements suggest that DN1p activity in the morning can drive locomotor activity, while the relative silence of the DN1p in the evening may have a permissive role on other cells controlling evening behavior.

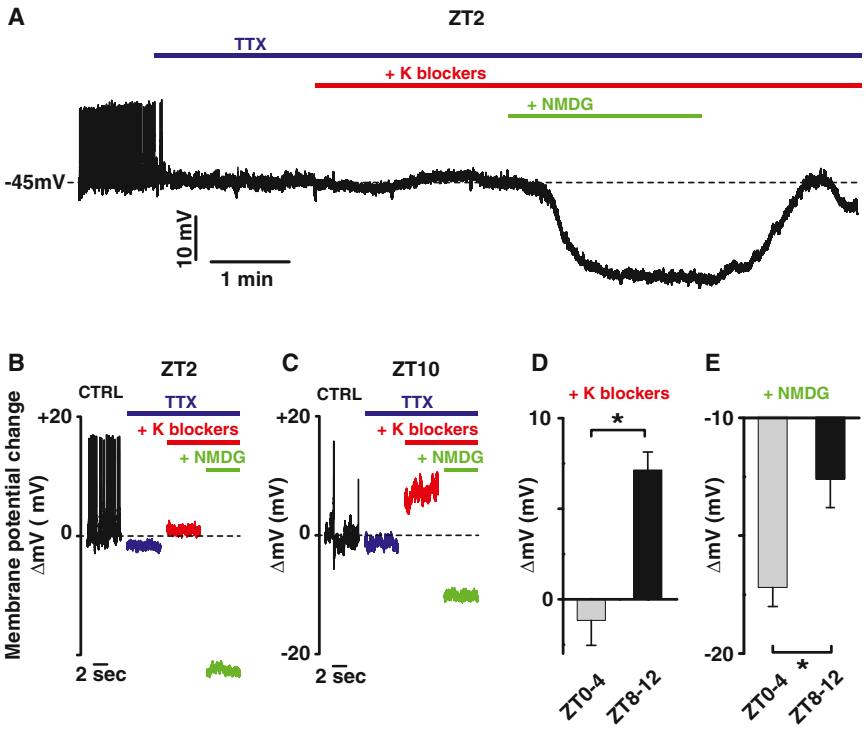

Figure 2. Time-of-Day-Dependent Effects of Resting K and Sodium Leak Conductance Blockade on Membrane Potential in DN1p Neurons

(A–C) (A) Representative current-clamp recording at ZT2 showing the effect of K and sodium conductance blockers on membrane potential. Bars indicate when drugs were applied (blue, TTX 10 μM; red, TEA 10 mM, 4-AP 5 mM, CsCl 2 mM; green, NMDG to replace the sodium from the extracellular solution). The effect of K blockers and sodium replacement on the membrane potential at different times of day are shown in (B) for ZT2 and (C) for ZT10.

(D and E) (D) Averaged changes of the membrane potential by K blockers (10 mM TEA, 5 mM 4-AP, and 2 mM CsCl): −1.2 ± 1.4 mV, n = 5 between ZT0–4 and 7.1 ± 1 mV, n = 5 between ZT8–12 and (E) sodium replacement with NMDG: −17.2 ± 0.8 mV, n = 5 between ZT0–4 and −12.6 ± 1.2 mV, n = 5 between ZT8–12. Results are expressed as mean ± SEM. Asterisks indicate statistical significance ($p < 0.05$) from t test.

To identify ionic conductances responsible for the resting membrane potential (RMP) rhythm, we blocked action potential firing using the voltage-dependent sodium channel blocker tetrodotoxin (TTX, 10 μM) and then applied a cocktail of potassium (K) channel inhibitors (10 mM TEA, 5 mM 4AP, and 2 mM CsCl) to block both voltage-dependent and voltage-independent (leak) K conductances (Fogle et al., 2011). We subsequently used N-methyl-D-glucamine (NMDG) substitution of extracellular sodium to block sodium leak currents (Jackson et al., 2004; Lu et al., 2007; Raman et al., 2000) at different times of day. As in mammals (Kuhlman and McMahon, 2004) and mollusks (Michel et al., 1993), the effect of blocking K leak conductances in *Drosophila* was dependent on time of day, producing little change in the morning (Figures 2A, 2B, and 2D) but a sizable depolarization in the evening (Figure 2C and 2D), indicating that rhythmic resting K conductance is conserved between flies and mammals (Kuhlman and McMahon, 2006). In contrast to K blockade, we discovered that blockade of resting sodium leak produced a larger hyperpolarization in the morning (Figures 2A and 2B–2E) than in the evening (Figures 2C–2E). Such time-of-day-dependent effects of sodium channel blockade have not been previously reported. Notably, this time-of-day-dependent effect on membrane potential of sodium blockade (Δ∼7 mV morning versus evening) is roughly equal to that of potassium blockade, suggesting that each makes a comparable contribution to daily excitability rhythms. As these rhythms are observed during network silencing from TTX, this suggests that changes in RMP are not driven by synaptic inputs but are intrinsic to the cells. Taken together, our results demonstrate that time-of-day-dependent sodium and K conductances, in the morning and evening, respectively, may underlie RMP rhythms.

The Ion Channel NARROW ABDOMEN Controls *Drosophila* Circadian Pacemaker Rhythms

A candidate mediator of resting sodium conductances in clock neurons and circadian behavior is the NARROW ABDOMEN (NA) ion channel (Lear et al., 2005; Nash et al., 2002). NALCN, the closely conserved mammalian homolog of NA, has been characterized as a voltage-independent mixed cation channel important for setting RMP and mediating resting leak sodium current (Lu et al., 2007; Swayne et al., 2009). This current is not blocked by TTX but can be reduced by either Gd^{3+} or replacement of extracellular sodium with NMDG (Lu et al., 2007). In a 12 hr LD cycle, increases in locomotor activity in advance of lights-on (i.e., morning anticipation) and lights-off (i.e., evening anticipation) are suppressed in na^{har} mutants (Lear et al., 2005; Nash et al., 2002). Although NA expression in the DN1p can rescue morning and, to a lesser extent, evening phenotypes (Zhang et al., 2010a), it remains unclear whether NA is a rhythmic mediator of resting membrane potential of circadian clock neurons. We therefore examined clock neuron excitability in *na* mutant DN1p neurons. Strikingly, na^{har} mutant DN1p neurons were completely silent (Figures 3A and 3B) and remained hyperpolarized throughout the whole day (Figure 3C and Table S1B). No daily rhythm in cellular excitability was detected in na^{har} (Figure 3D and Table S2C; $p > 0.35$). Positive current injections show that na^{har} mutant neurons fire fewer action potentials compared to controls, indicating that these neurons are healthy and can still generate action potentials but require more depolarizing current to fire at the same rate as *WT* neurons (Figures 3D and 3E). Wild-type membrane excitability can be restored by inducing NA expression only in the DN1p in the mutant, confirming that these effects are due to *na* and are likely cell autonomous

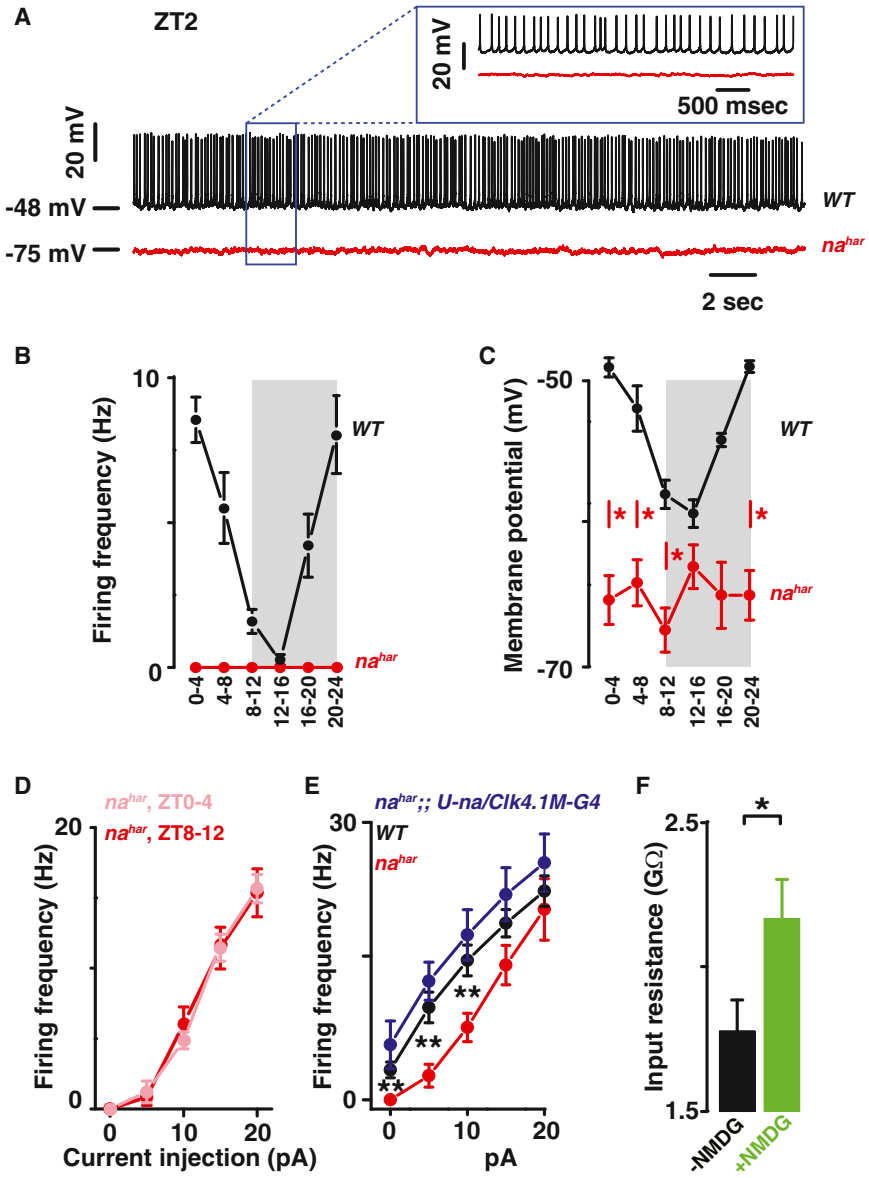

Figure 3. The Ion Channel Narrow Abdomen Controls *Drosophila* Circadian Pacemaker Neuronal Rhythms

(A–C) (A) Representative current-clamp recordings at ZT2 showing that the na^{har} DN1p neurons (red) are hyperpolarized and silent compared to *WT* DN1p neurons (black). Statistical analysis comparing the firing frequency (B) and membrane potential (C) of the *WT* (black) and na^{har} (red) DN1p neurons. Red asterisks indicate statistical significance between *WT* and na^{har} neurons ($p < 0.05$, from a one-way ANOVA, Tukey's post hoc test). (Data for *WT* neurons are also depicted in Figures 1B and 1C).

(D) Depolarizing current injections confirm the lack of detectable rhythms in cellular excitability in the na^{har} neurons (light red, ZT0–4; dark red, ZT8–12, $p > 0.35$).

(E) The decrease in cellular excitability can be restored by rescuing the expression of NA only in the DN1p in the mutant: *WT* (black), na^{har} (red) and na^{har};; *U-na/Clk4.1M-G4* (blue) DN1p neurons.

(F) Histograms showing that sodium substitution with NMDG induces an increase in the input resistance, indicating that NA is open at rest (black and green columns are before and after NMDG substitution, respectively). Results are expressed as mean ± SEM. Asterisks indicate statistical significance (t test, $p < 0.05$).

See also Tables S1 and S2.

(Figure 3E and Table S2D). NMDG substitution induces an increase in the input resistance, indicating that NA is open at rest (Figure 3F).

We next directly measured voltage-clamped NA-dependent current (I_{NA}) at different times of day. A voltage ramp protocol (from –113 mV to +87 mV) was used to measure the inward current at −113 mV, in the presence of TTX. Replacing the sodium from the extracellular solution with NMDG reveals the sodium leak current (Figure 4A). Consistent with the sodium leak current being driven specifically by NA, the observed current is reduced in the na^{har} mutant neurons and can be restored by rescuing the expression of NA in the mutant (Figure 4A). Measuring I_{NA} at different times of day reveals a diurnal modulation of current density: it is higher in the morning and lower in the evening (Figures 4B and 4C and Table S1D). No rhythm is detected in the na^{har} (Figures 4B and 4C and Table S1D) or in per^{01} mutants (Figure 4D, $p = 0.21$), the latter indicating core clock control. Further, the rhythm in NA conductance was evident even after Clk4.1M-GAL4-driven rescue (Figure 4E). Given GAL4 stability, any promoter-driven transcriptional rhythms may not be evident as GAL4 protein rhythms, and thus GAL4-induced transcription of *na* may not be rhythmic (Kaneko et al., 2000), suggesting that NA current rhythms do not require *na* transcript rhythms. Taken together, these results indicate that the clock control of sodium leak current through NA mediates rhythms of resting membrane potential.

Nlf-1 Expression is Time Dependent and Is Required for Locomotor Activity Rhythms and NA Leak Current

To identify molecular links between core clocks and membrane excitability, we employed fluorescence-activated cell sorting of GFP-labeled DN1p and performed RNA-Seq at distinct times during the LD cycle. Using empirical JTK_CYCLE (Hutchison et al., 2015), an updated version of JTK_CYCLE (Hughes et al., 2010), to detect rhythmic transcripts at a false discovery rate of 5% (Benjamini-Hochberg adjusted, $p < 0.05$), we observed robust 24 hr rhythms in CG33988, the fly ortholog of the NCA localization factor 1 (NLF-1), but not in *na* itself, its regulatory subunits *unc79* and *unc80* (Lear et al., 2013), nor the NALCN

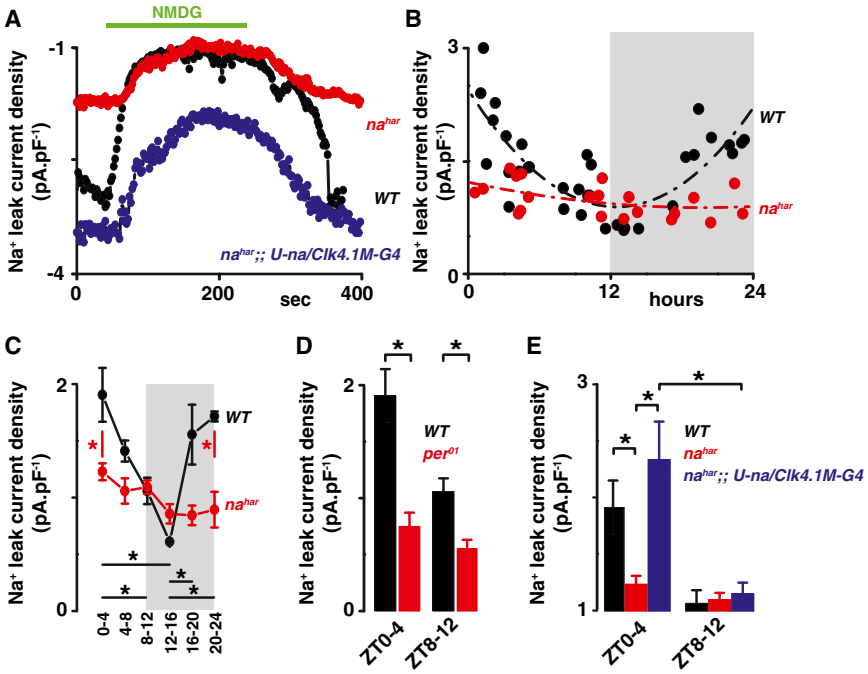

Figure 4. The Sodium Leak Current Is under Clock Control in *Drosophila* Circadian Pacemaker Neurons

(A) Representative time courses showing the sodium leak current (I_{NA}) recorded at −113 mV from a ramp protocol in *WT* (black), na^{har} (red), and na^{har}*;; U-na/Clk4.1M-G4* (blue) DN1p neurons.

(B) All recorded *WT* neurons (black dots) and na^{har} neurons (red dots) are plotted against time of day for sodium leak current (I_{NA}).

(C) Quantification and statistical analysis are shown. Gray areas represent the dark phase of the LD cycle. Red asterisks indicate statistical significance between *WT* and na^{har} neurons, and black asterisks indicate statistical significance between different time points in *WT* neurons ($p < 0.05$) from a one-way ANOVA, Tukey's post hoc test.

(D) Histograms showing the NA current in *WT* (black) and per^{01} (red) DN1ps recorded at different times of day ZT0–4 versus ZT8–12 (for per^{01}, $I_{NA} = 0.7 \pm 0.2$ pA.pF^{-1}, n = 8 at ZT0–4 and 0.5 ± 0.1 pA.pF^{-1}, n = 7 at ZT8–12). Asterisks indicate statistical difference between *WT* and per^{01}, $p < 0.05$ from t test.

(E) Histograms showing the sodium leak current in *WT* (black), na^{har} (red), and na^{har}*;; U-na/Clk4.1M-G4* (blue) DN1p neurons at different times of day (ZT0–4 versus ZT8–12) (for na^{har}*;; U-na/Clk4.1M-G4,* $I_{NA} = 2.3 \pm 0.3$ pA.pF^{-1}, n = 4 at ZT0–4 and 1.1 ± 0.1 pA.pF^{-1}, n = 4 at ZT8–12). Results are expressed as mean ± SEM. Asterisks indicate statistical significance ($p < 0.05$) from a t test.

activators such as Src family kinases (Lu et al., 2009), *Src42a*, and *Src64b* in flies (Figure 5A). NLF-1 has been previously shown to interact with NA orthologs in worms (NCA-1 and -2) and mammals (Xie et al., 2013). NLF-1 protein is expressed in the endoplasmic reticulum and is required for the proper axonal localization of NCA-1 and -2 (Xie et al., 2013). Rhythmic expression of *CG33988/Nlf-1* transcript was further confirmed with quantitative PCR (Figure 5B), and consistent with clock control, *CG33988/Nlf-1* transcript is rhythmic in the DN1p in constant darkness (DD) (Figure 5C). *Nlf-1* transcript is also highly enriched in the DN1p clock neurons in comparison to whole heads (Figure 5D). Chromatin immunoprecipitation experiments indicate that the core clock transcription factor CLOCK rhythmically binds the *Nlf-1* genomic locus, suggesting a direct biochemical link to the core clock (Abruzzi et al., 2011). Taken together, this suggests that *Nlf-1* is a key mediator of NA rhythms that couples the transcriptional oscillator to membrane potential rhythms.

To assess the function of NLF-1 in circadian behavior, we knocked down its transcript levels using three independent transgenic dsRNA and shRNA lines in combination with the broad circadian driver *tim*-GAL4. In contrast to the previously reported weak effect of CG33988 RNAi knockdown on evening behavior (Ghezzi et al., 2014), we found dramatic reductions in rhythmic strength in DD (3/3 lines) and reduced anticipation of lights-on (2/3 lines) and lights-off transitions (3/3 lines) under LD conditions (Figures 6A and S3). These effects are comparable to those observed in loss-of-function *na* alleles (Lear et al., 2005) and knockdown of *na* using RNAi (Figure S3 and Tables S3 and S4). Restricting *Nlf-1* knockdown to non-PDF clock neurons (*tim*-GAL4, *pdf*-GAL80) also caused reduced morning and evening anticipation, as well as reduced rhythmicity (Tables S3 and S4), consistent with prior *na* rescue studies (Lear et al., 2005). Further restricting *Nlf-1* knockdown to the DN1p using Clk4.1M-GAL4 resulted in reduced DD rhythmicity (Table S3).

The role of *Nlf-1* extends to PDF neurons. Restricting *Nlf-1* knockdown to PDF neurons, using two different *pdf*-GAL4 drivers (*pdf*-GAL4 and *pdf0.5*-GAL4 [Park et al., 2000]), dramatically reduces free running rhythms (Table S3), consistent with the highly enriched *Nlf-1* transcript observed in larval PDF+ sLNv neurons (Nagoshi et al., 2010) and with the described role of NA in PDF neurons (Lear et al., 2005). In addition, we extended our patch-clamp analysis to the large LNv neurons (Figure S4A). Here, we observed clock-dependent rhythms in membrane properties as previously observed (Figures S4B and S4C) (Cao and Nitabach, 2008; Sheeba et al., 2008). In addition, we found clock-dependent NA current rhythms similar to those we observed for the DN1p, with peak levels in the morning (Figure S4D). Thus, our findings in DN1p extend to other circadian neurons.

We then tested whether *Nlf-1* is important for NA current levels, which may reflect the proper channel localization to the cell membrane. Knockdown of *Nlf-1* expression was confirmed in the DN1p with quantitative PCR (Figure 6B). We find that knockdown in the DN1p results in a similar phenotype to that observed for *na* mutants with cells becoming hyperpolarized and silent (Figure 6C). Cellular excitability is also decreased in the *Nlf-1* knockdown, as the neurons are less responsive to depolarizing currents (Figure 6D and Table S2E). NA-dependent current was also strongly suppressed after *Nlf-1* knockdown (Figure 6E).

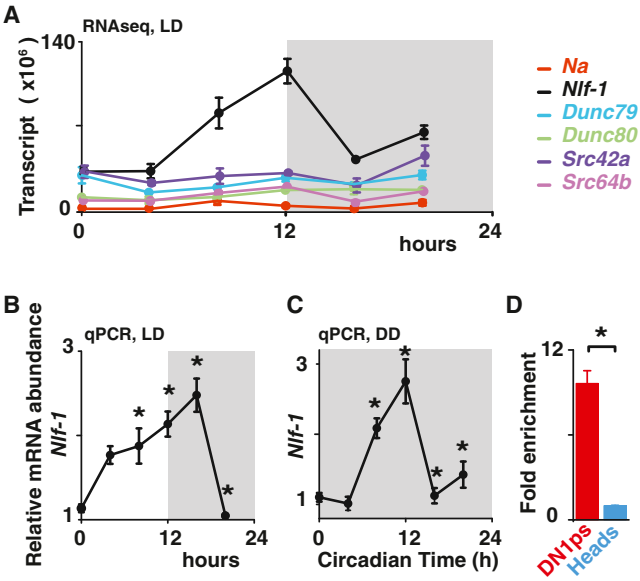

Figure 5. *Nlf-1* Is Rhythmically Expressed in DN1p Neurons

(A–D) (A) *Nlf-1* mRNA shows rhythmic expression using RNA-seq data from FACS-sorted DN1p neurons in LD (for isoform RB, shown in graph, BH corrected p = 0.005). *na*, *Unc79*, *Unc80*, *Src64B*, and *Src42a* are not robustly cycling (graph shows isoforms with highest expression: BH = 0.28 for *na-RF*, 0.2 for *Dunc79-RE*, 0.85 for *Dunc80-RE*, 0.71 for *Src42a-RA*, and 0.07 for *Src64B-RJ*). *Nlf-1* cycles under LD (B) and during the first day of constant darkness (DD1) conditions (C) in DN1ps using qPCR. Based on two independent experiments, an asterisk indicates differences statistically significant one-way ANOVA, Tukey's post hoc test, LD ZT0 versus ZT12 p = 0.0011, ZT0 versus ZT16, p = 0.000142, ZT4 versus ZT16 p = 0.029, ZT0 versus ZT8 p = 0.022, ZT12 versus ZT20, p = 0.000441, ZT16 versus ZT20 p = 0.000136. DD1 CT0 versus CT8 p = 0.01081, CT0 versus CT12 p = 0.000142, CT12 versus CT16 p = 0.000145 and CT12 versus CT20 p = 0.000459. (D) *Nlf-1* expression is enriched in the DN1ps versus whole head (t test, p < 0.02). Results are expressed as mean ± SEM.

To further examine the mechanism by which NLF-1 might regulate NA, we assayed NA protein expression after *Nlf-1* knockdown. *Nlf-1* knockdown with a broad neuronal driver (elav-G4) also results in strong reductions in rhythmic strength in DD and reduced morning and evening anticipation (Figure S5A and Tables S3 and S4). Surprisingly, NA protein levels were dramatically reduced in these flies (Figure S5B). We also observed lower NA expression (~50% reduction) when *na* was driven transgenically in the DN1p of *Nlf-1* knockdown flies (Figure S5C). In part due to the small soma and limited expression in projections, we could not reliably assess cell membrane or axonal localization. Yet *Nlf-1* knockdown does not reduce DN1p *na* transcript levels (Figure S5D). *Nlf-1* knockdown in the DN1p phenocopies a *na* mutant, suggesting that NA current is nearly abolished (Figure 6E) yet transgenic NA is reduced by just ~50%. Thus, we favor the view that strong effects of *Nlf-1* knockdown on NA current are only in part due to changes in NA levels.

If the oscillation of *Nlf-1* transcript is critical to setting NA levels and DN1p membrane excitability, we would predict that *Nlf-1* overexpression would increase NA current at evening time points when NA current is typically at trough levels. We observed that, in the evening (ZT8–12) NLF-1 overexpression depolarizes membrane potential, elevates firing rates (Figure 6F) and cellular excitability (Figure 6G and Table S2F), and, most importantly, increases NA current (Figure 6H) at a time when each of those parameters is near their daily trough in wild-type flies. Indeed, sodium leak current density in the evening in *Nlf-1* overexpression flies (~2pA.pF^{-1}) is comparable to that seen at peak levels in wild-type flies in the morning. Taken together, these results indicate that *Nlf-1* expression is rhythmic and mediates NA activity rhythms. This demonstrates a molecular mechanism linking the core clock to membrane excitability via the rhythmic transcription of a factor important for ion channel function in *Drosophila* circadian neurons (Figure 6I).

NALCN Current Is under Clock Control in Mammalian SCN Pacemaker Neurons

Although we demonstrated a rhythmic function for resting sodium leak in *Drosophila* clock neurons, rhythmic resting sodium conductances have yet to be described in mammalian clock neurons. Previous patch-clamp analyses of dissociated SCN neurons demonstrated the presence of a NALCN-like current (TTX-resistant, NMDG-sensitive, voltage-independent sodium conductance termed $I_{background}$) that is largely responsible for the initial phase of the depolarizing drive during the interspike interval (Jackson et al., 2004). To determine whether this activity is rhythmic in mammalian circadian pacemaker neurons, we performed voltage-clamp analysis during subjective day and night from organotypic slices containing the SCN from mice entrained for 2 weeks in LD and then maintained under constant darkness conditions for at least 3 weeks. Rhythms in firing frequency, membrane potential, and input resistance were observed, thus validating the preparation (Figures S6A–S6C). In the presence of TTX to block action potentials, the NALCN blockers, NMDG (Figure 7A) or Gd^{3+} (Figure S6D), induce a hyperpolarization, while no additional effect of applying Gd^{3+} after sodium replacement with NMDG was observed (Figure 7B). Importantly, in hippocampal neurons, the vast majority of current with this pharmacological profile is mediated by NALCN (Lu et al., 2007).

To confirm the molecular identity of the sodium leak in the SCN, we generated a forebrain-specific knockout of NALCN with a CamkIIα-cre driver. With this driver, CRE expression mimics the endogenous expression of *CamkIIα* (enriched in the forebrain, neuron-specific [Casanova et al., 2001]). *CamkIIα* expression is also highly enriched in the SCN, and loss of circadian rhythms in mice with a CamkIIα-specific knockout of a core clock gene (*Bmal1*) is observed (Izumo et al., 2014). We first confirmed that the NMDG-evoked hyperpolarization (Figure 7A) is greatly reduced in the *CamkIIα−Cre;NALCN$^{fx/fx}$* animals compared to age-matched sibling controls (Figures 7C and 7D, p = 0.005). Consistent with a role of NALCN in controlling the membrane potential and firing frequency of neurons, *CamkIIα−Cre;NALCN$^{fx/fx}$* SCN neurons were hyperpolarized and silent (Figures S6E and S6F, p < 0.007). Importantly, a small depolarization current injected into the *CamkIIα−Cre;NALCN$^{fx/fx}$* SCN neurons was able to evoke strong firing (Figure S7G), indicating that cells were healthy but required a greater depolarizing input to evoke action potentials. We further confirmed the presence of NALCN current during the interspike interval in

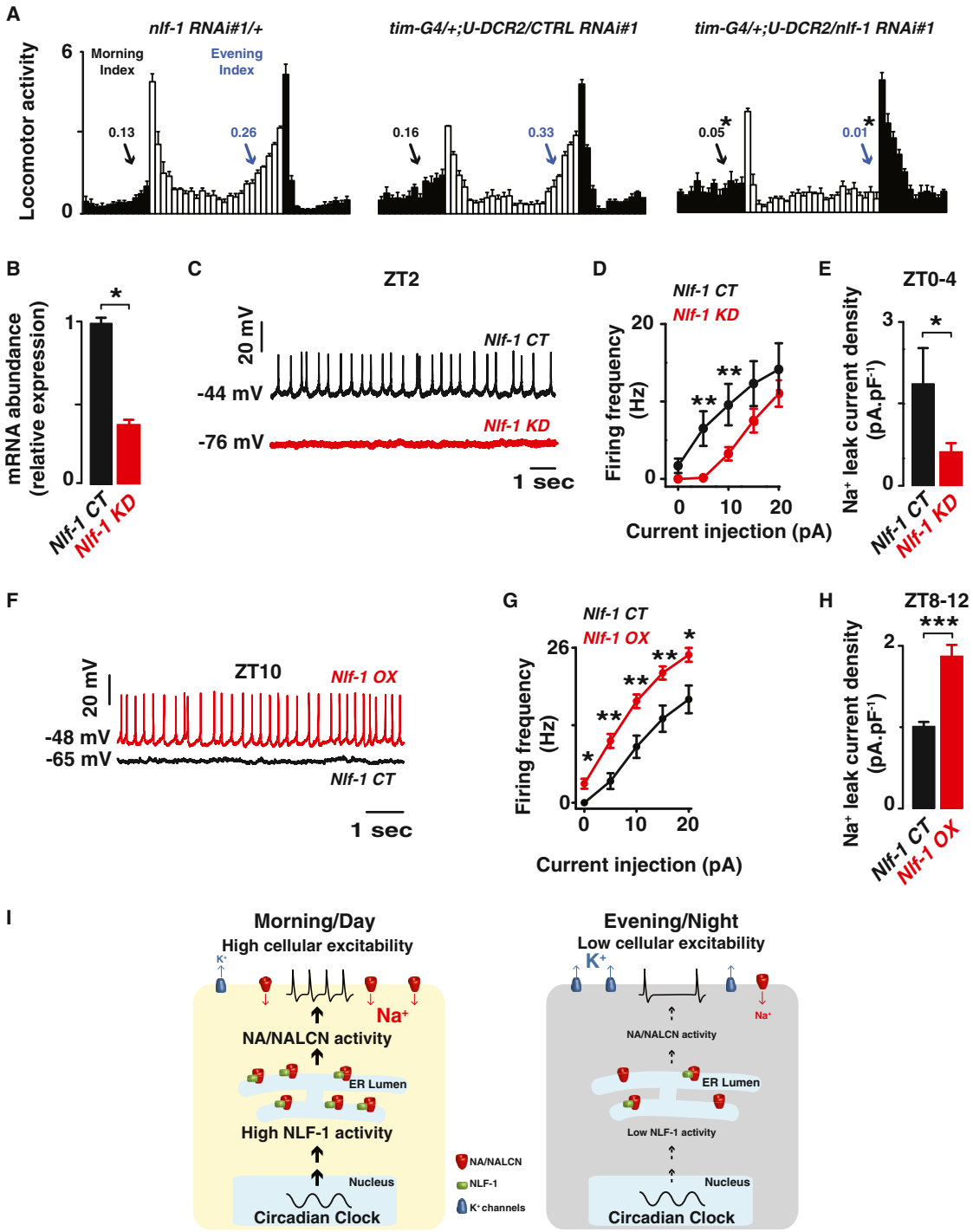

Figure 6. *Nlf-1* Is Required for Anticipatory Behavior and NA Current

(A) *Nlf-1* RNAi-expressing flies (*tim-G4/+; U-Dcr2/Nlf-1 RNAi#1*) show reduced morning anticipation (Morning Index) and evening anticipation (Evening Index) under LD conditions when compared to genetic controls (*Nlf-1 RNAi#1/+* and *tim-G4/+; U-Dcr2/CTRL RNAi#1*) (t test, $p < 0.05$).

(B) *Nlf-1* expression is reduced in the DN1ps of *Nlf-1* RNAi-expressing flies (t test, $p < 0.05$).

(C) Representative current-clamp recordings at ZT2 showing that the *Nlf-1* knockdown DN1p neurons (red) are hyperpolarized and silent compared to control DN1p neurons (black).

(D) Depolarizing current injections confirm the decrease in cellular excitability in *Nlf-1* knockdown neurons (red) versus control (black) ($p < 0.05$).

(E) Sodium leak current density is dramatically reduced in the *Nlf-1* knockdown neurons (red) versus control neurons (black) (1.9 ± 0.7 pA.pF^{-1}, n = 4 in *Nlf-1 CT* and 0.6 ± 0.2 pA.pF^{-1}, n = 5 in *Nlf-1 KD*, measured at ZT0-4, $p < 0.05$).

(legend continued on next page)

organotypic slices containing the SCN with pharmacology: NMDG and Gd^{3+} sensitive. No additional block by Gd^{3+} was observed after NMDG application (Figures S6H and S6I). This NMDG-sensitive inward current was greatly reduced in the *CamkIIα-Cre;NALCN*$^{fx/fx}$ SCN neurons (Figures 7E and 7F, p = 0.002). Taken together, these data indicate that the vast majority of the sodium leak flowing during the interspike interval in SCN neurons is carried by NALCN (I_{NALCN}), consistent with other mammalian neurons (Lu et al., 2007). We then assessed I_{NALCN} at different times of day and found that it was significantly larger during the subjective day than subjective night, consistent with a control by the circadian clock (Figure 7G, p < 0.001).

To determine the impact of a day-night change in I_{NALCN} (~0.7 pA.pF^{-1}) on firing frequency and membrane potential, we simulated sodium leak current modulation using an updated version of a mathematical model of SCN membrane excitability (Diekman et al., 2013) (see Experimental Procedures). This model accurately captures the effect of NALCN blockers on the membrane potential of SCN neurons (Figure 7H). According to this model, modest daily changes in sodium leak conductance comparable to those observed experimentally can have sizable effects on neuronal firing rates (Figure 7I). To explore the contributions of both sodium and potassium leak currents to the daily variation of firing rate in SCN neurons, we simulated concurrent modulation of these two conductances. Beginning from a subjective day firing rate of 7 Hz, reducing sodium leak conductance by the amount suggested by our experimental measurements (~0.7 pA.pF^{-1}, Figure 7G) decreases firing rate to 2 Hz. Experimentally, we observed that, during the subjective day, I_{NALCN} is, in fact, positively correlated with firing frequency (Figure S6J), suggesting that I_{NALCN} significantly impacts neuronal physiology. Even lower firing rates that are characteristic of subjective night (0.5 Hz) can be achieved by increasing potassium leak conductance in conjunction with this reduction in sodium leak (Figures 7J and S7). Thus, elevated sodium leak during the day and elevated potassium leak at night can recapitulate the experimentally observed daily variations in SCN firing rate through relatively modest changes in these leak currents.

DISCUSSION

Taken together, our work defines a conserved mechanism for the maintenance of circadian oscillations necessary for robust daily behaviors (Figure 6I) that we term the "bicycle" model. Membrane oscillations are driven by two cycles with opposite temporal phases analogous to cycling bicycle pedals. During the morning/day, sodium leak mediated by NA/NALCN is elevated while resting K currents are reduced, depolarizing the neuron to promote elevated firing rates. During the evening/night, sodium leak is low and resting K currents are elevated, hyperpolarizing the cell to suppress firing rates. The clock-controlled transcript *Nlf-1* drives the rhythm of NA/NALCN current, linking the core clock to ion channel activity.

While *Drosophila* has been a well-established model for defining molecular genetic mechanisms, relatively little is known about the specific ionic currents that underlie fly pacemaker neuron excitability rhythms due to the small size of *Drosophila* soma. Most cellular electrophysiological analyses have focused on the largest cells, the large ventral lateral neurons (Cao and Nitabach, 2008; Fogle et al., 2011, 2015; Sheeba et al., 2008). Yet, even in these neurons, the specific ionic currents under clock control have yet to be defined. Using whole-cell, patch-clamp electrophysiology of DN1p pacemaker neurons, we found high-amplitude oscillations of spontaneous firing rates and basal membrane potential that are comparable to those observed in mammalian SCN clock neurons. Moreover, we demonstrate clock control of both resting sodium leak conductance as well as resting potassium conductance. Our data suggest that the patch-clamp analysis of the DN1p will be valuable in defining the ionic currents that mediate clock control of neuronal excitability.

Our data indicate that the daily changes in membrane excitability that we observe are cell autonomous. The observed cycles of resting currents are evident even in the presence of TTX. Bath application of TTX silences neurons and thus would block firing-dependent neurotransmitter release. Moreover, cycling sodium leak currents are driven by the transcriptional oscillation of *Nlf-1*, providing a cell-autonomous mechanism for clock control. We propose that cell-autonomous clock regulation collaborates with rhythmic network inputs, such as PDF, which likely act in the morning to excite DN1p neurons (Kunst et al., 2014; Seluzicki et al., 2014). In turn, DN1p excitation drives waking behavior in the morning (Kunst et al., 2014; Zhang et al., 2010a, 2010b) and free running rhythmicity, perhaps via the DH44 neurons in the pars intercerebralis (Cavanaugh et al., 2014). As the DN1p are also important for evening behavior (Zhang et al., 2010a), evening silencing may permit other neurons (e.g., the LNd) to drive evening behavior.

The clock control of membrane potential has largely focused on modulation of resting potassium conductance in the SCN (Kuhlman and McMahon, 2004) as well as in *Bulla* photoreceptors (Michel et al., 1993; Michel et al., 1999). Surprisingly, we observed rhythms of sodium leak conductance in the fly

(F) Representative current-clamp recordings at ZT10 showing that the *Nlf-1* overexpressing DN1p neurons (red) are depolarized and more active compared to control DN1p neurons (black).
(G) Depolarizing current injections confirm the increase in cellular excitability in *Nlf-1*^{V5}-overexpressing neurons (red) versus control (black) (p < 0.05).
(H and I) (H) Sodium leak current density is also increased in the *Nlf-1*^{V5}-overexpressing neurons (red) versus control neurons (black) (1 ± 0.05 pA.pF^{-1}, n = 4 in *Nlf-1 CT* and 1.9 ± 0.1 pA.pF^{-1}, n = 5 in *Nlf-1 OX*, measured at ZT8–12, p < 0.05). Results are expressed as mean ± SEM. Asterisks indicate statistical significance (p < 0.05 from a t test). A summary cartoon depicting the conserved bicycle model for controlling membrane excitability of circadian pacemaker neurons is shown in (I). In the morning/day, the molecular clock drives high NLF-1 activity, increasing the sodium leak activity, and K conductances are reduced, thus increasing cellular excitability. In the evening/night, the sodium leak is decreased, and, in parallel, K conductances are high, thus silencing the neurons. This dual regulation of the conductances responsible for the membrane properties is critical for driving high-amplitude rhythmic oscillations of cellular excitability.
See also Figures S3, S4, and S5 and Tables S2, S3, and S4.

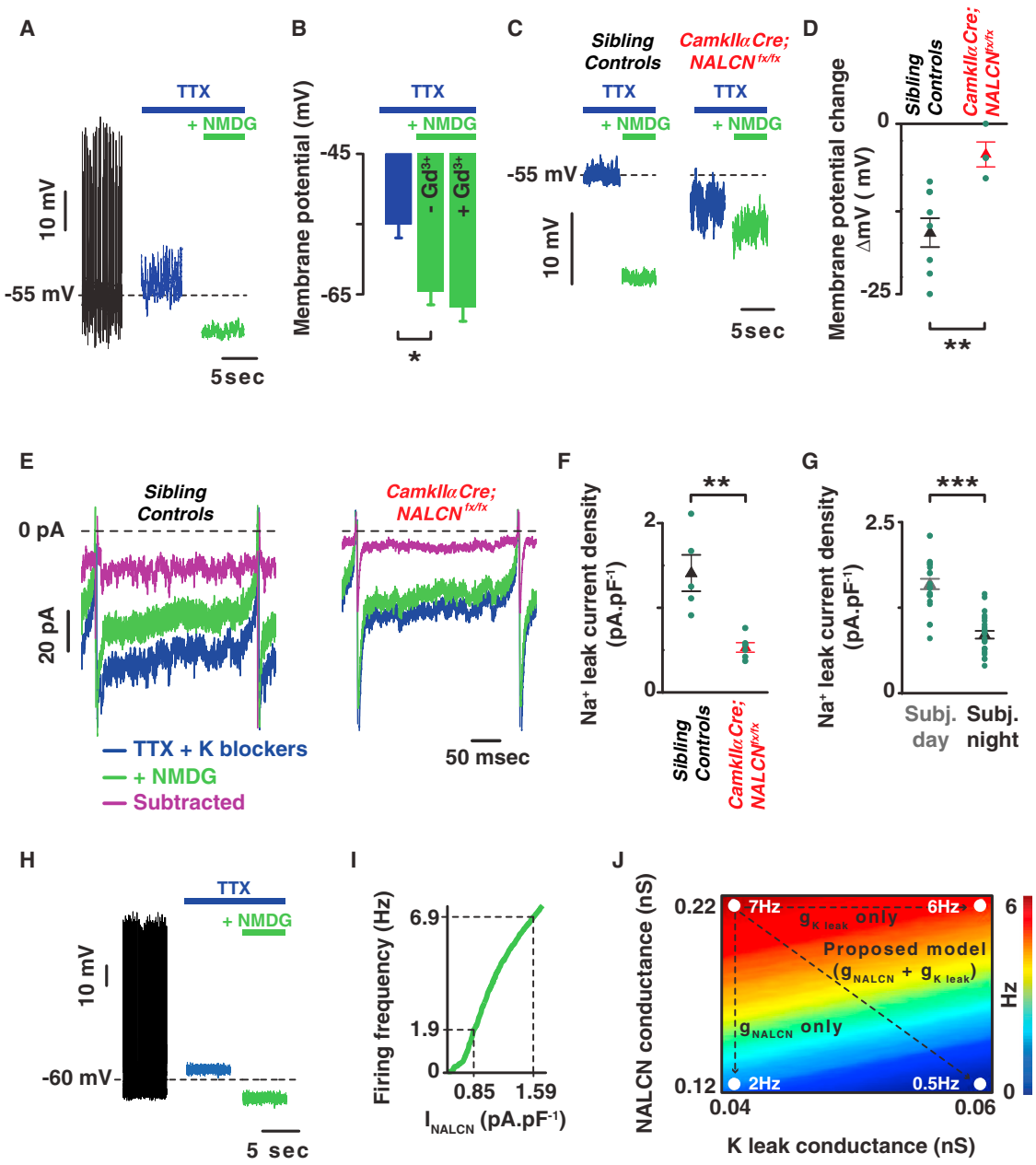

Figure 7. NALCN Current Is under Clock Control in Mammalian SCN Pacemaker Neurons

(A) Representative current-clamp recording showing the role of the TTX-resistant sodium leak (difference between green and blue) in setting the membrane potential of mammalian SCN neurons.

(B) NMDG hyperpolarizes the cell with no additional effect in the presence of Gd^{3+}.

(C) NMDG-evoked hyperpolarization was reduced in a brain-specific knockout of NALCN.

(D) Quantification and statistical analysis of the NMDG-evoked hyperpolarization is shown: −15.9 ± 2.0 mV, n = 9 in controls (black triangle) and −4.5 ± 1.7 mV, n = 4 (red triangle). Asterisks indicate statistical significance (t test, p = 0.005).

(E) Action potential clamp recordings showing the sodium leak flowing during the interspike interval in SCN neurons from sibling control (left) and *CamkIIa-Cre;NALCN$^{fx/fx}$* animals (right). In the presence of TTX and K blockers (blue trace), the sodium leak current flowing during the interspike interval (I_{NALCN}) was reduced after sodium substitution with NMDG (green trace). The sodium leak current (I_{NALCN} = subtracted = purple trace) was revealed by subtracting the inward current in the presence of NMDG from the inward current present with TTX and K blockers.

(F) I_{NALCN} was reduced in *CamkIIa-Cre;NALCN$^{fx/fx}$* compared to sibling controls animals (0.5 ± 0.1 pA.pF^{-1}, n = 6 in *CamkIIa-Cre;NALCN$^{fx/fx}$* [red triangle] and 1.4 ± 0.2 pA.pF^{-1}, n = 5 in sibling controls [black triangle]). Asterisks indicate statistical significance (t test, p = 0.002).

(G) Circadian variation of I_{NALCN}: 1.6 ± 0.1 pA.pF^{-1}, n = 25 during the subjective day (gray columns) and 0.8 ± 0.1 pA.pF^{-1}, n = 23 during the subjective night (black columns). Asterisks indicate statistical significance (t test, p < 0.001). Green dots represent individual cells.

(legend continued on next page)

DN1ps and l-LNvs, as well as in mammalian SCN, that are mediated by the NA/NALCN channel. This sodium leak exhibits the pharmacological sensitivity previously defined for the NALCN current (Lu et al., 2007), most notably $NMDG^+$ and Gd^{3+} block. In addition, the current is reduced in *na* mutant flies and in mice with a brain-specific knockout of NALCN. Clock modulation of this sodium current also likely impacts neurophysiology. Loss-of-function *na* mutants and NALCN knockout result in silent and hyperpolarized neurons. Computational modeling of SCN neurons demonstrates that the modest daily rhythm of sodium leak can significantly impact overall firing rates. Thus, our work defines a molecular mechanism for clock control of membrane excitability.

Using a combination of genomics, electrophysiology, and behavior, our work reveals a molecular pathway that links the transcriptional clock to these sodium current rhythms. The mechanisms of clock control of membrane excitability have largely focused on the direct clock control of ion channel transcripts (Itri et al., 2005; Kudo et al., 2011; Meredith et al., 2006; Nahm et al., 2005; Pennartz et al., 2002; Pitts et al., 2006). Using RNA-seq and qPCR validation on FACS-sorted DN1p neurons, we identify robust rhythms of *Nlf-1*, an ER protein that is important for the localization of NALCN and its orthologs (Xie et al., 2013). Moreover, RNAi knockdown of *Nlf-1* results in suppression of behavioral rhythms, NA expression, and related current. Conversely, NLF-1 overexpression increases NA current, firing frequency, and membrane potential in the evening when these parameters are typically at their troughs in wild-type flies, suggesting that *Nlf-1* controls activity and/or localization of NA. Chromatin immunoprecipitation has demonstrated rhythmic CLK binding at the *Nlf-1* locus (Abruzzi et al., 2011). Our cell-specific knockdown experiments indicate that *Nlf-1* functions broadly within the clock network to control morning and evening anticipation as well as DD rhythms, suggesting that this mechanism is widely applied. Future work will be required to determine whether *Nlf-1*/NA rhythms in morning and evening cells have distinct phases. Nonetheless, we have defined a molecular pathway that directly links CLK-driven transcriptional oscillations to NA current and behavioral rhythms.

This mechanism may not only be operating in clock neurons but may also be broadly involved in rhythmic changes in brain states. For instance, NALCN is critical to the maintenance of respiratory rhythms (Lu et al., 2007). Both fly and worm *na*/*nca* loss of function results in disrupted locomotion as well as altered sensitivity to general anesthetics (Humphrey et al., 2007). *na* mutant flies also show altered behavioral state transitions related to sleep and anesthesia (Joiner et al., 2013). More generally, the NA/NALCN current shown here has an identical electrophysiological profile to the tonic cation current required for regular firing in neurons of the mouse cerebellar nuclei (Raman et al., 2000).

Our work also demonstrates that, like the core molecular clock, clock control of membrane potential is also widely conserved in neurons important for sleep and wake. We hypothesize that the common ancestor of the mouse and the fly had master circadian pacemaker neurons that drove its daily behavior. Moreover, these clock neurons employed daily antiphase sodium and potassium conductances to drive their rhythmic activity. Thus, our finding suggests an ancient strategy governing neuronal activity important for driving daily cycles of sleep and wake.

EXPERIMENTAL PROCEDURES

Please see the Supplemental Experimental Procedures for detailed protocols.

Electrophysiological Recordings from *Drosophila* Neurons

Whole-brain electrophysiology experiments were performed with pipettes (10–14 MΩ) filled with internal solution. The sodium leak current (I_{Na}) was examined in the presence of TTX (10 μM), TEA (10 mM), 4-AP (5 mM), and CsCl (2 mM) and was revealed by replacing the extracellular sodium with NMDG (Lu et al., 2007). All recordings were corrected for liquid junction potential (13 mV). For analysis, cells with high series resistance or with low membrane resistance (< 1GΩ) were discarded.

RNA Isolation, Amplification, and Sequencing

RNA was isolated and amplified as previously described (Kula-Eversole et al., 2010). The quality and quantity of dsDNA was assessed on Bioanalyzer (Agilent). After quality control, libraries were generated using TruSeq Sample Preparation Guide (following manufacturer's protocol [Illumina]). The RNA-seq was performed on HiSeq2000 (Illumina). Bowtie (Langmead et al., 2009) was used to align short-read aligner to references (obtained from http://flybase.org). Quantification was performed using eXpress (Roberts et al., 2011). Rhythmic transcripts were detected using empirical JTK_CYCLE (Hutchison et al., 2015), and transcripts were considered robustly rhythmic when the Benjamini-Hochberg corrected p value or false discovery rate < 0.05. Empirical JTK_CYCLE derives p values empirically considering asymmetric waveforms.

Mathematical Modeling

Simulations of a Hodgkin-Huxley type model of SCN membrane excitability were performed using MATLAB R2012b (Mathworks). The model was fit to experimental data from SCN neurons and consists of a system of ordinary differential equations for membrane potential (V) and six ionic gating variables (m, h, n, r, f, and b):

$$C\frac{dV}{dt} = I_{app} - I_{Na} - I_K - I_{Ca} - I_{BK} - I_{Cl} - I_{K\ leak} - I_{NALCN}$$
$$= I_{app} - g_{Na}m^3h(V - E_{Na}) - g_K n^4(V - E_K) - g_{Ca}rf(V - E_{Ca}) - g_{BK}b(V - E_K)$$
$$- g_{Cl}(V - E_{Cl}) - g_{K\ leak}(V - E_K) - g_{NALCN}(V - E_{NALCN})$$

$$\frac{dx}{dt} = \frac{x_\infty(V) - x}{\tau_x(V)} \quad x = m, h, n, r, f, b$$

(H) Simulations showing the role of TTX-resistant sodium leak in setting the membrane potential using a mathematical model of SCN membrane excitability. Voltage traces from control simulation (g_{Na} = 229 nS, g_{NALCN} = 0.22 nS) and simulated application of TTX (g_{Na} = 0 nS) and NMDG (g_{NALCN} = 0 nS).

(I) The model predicts the magnitude of change in firing rate as a function of magnitude of change in NALCN current density (g_{NALCN} = 0.12 to 0.22 nS). A decrease of 0.74 $pA.pF^{-1}$ in I_{NALCN} (observed between the subjective day and night [G]) leads to a 5 Hz decrease in firing rate.

(J) Firing rate as a function of g_{NALCN} and $g_{K\ leak}$ in a model SCN neuron. Arrows: decreasing g_{NALCN} alone reduces firing rate from 7 Hz to 2 Hz, whereas increasing $g_{K\ leak}$ reduces firing rate from 7 Hz to 6 Hz. Concurrently decreasing g_{NALCN} and increasing $g_{K\ leak}$ reduces firing rate from 7 Hz to 0.5 Hz. Results are expressed as mean ± SEM.

See also Figures S6 and S7.

$$m_\infty = \frac{1}{1+\exp(-(V+35.2)/8.1)}, \quad h_\infty = \frac{1}{1+\exp((V+62)/4)},$$
$$n_\infty = \frac{1}{(1+\exp((V-14)/(-17)))^{0.25}}, \quad r_\infty = \frac{1}{1+\exp(-(V+25)/7.5)},$$
$$f_\infty = \frac{1}{1+\exp((V+260)/65)}, \quad b_\infty = \frac{1}{1+\exp(-(V+20)/2)},$$
$$\tau_m = \exp(-(V+286)/160), \quad \tau_h = 0.51+\exp(-(V+26.6)/7.1),$$
$$\tau_n = \exp(-(V-67)/68), \quad \tau_r = 3.1,$$
$$\tau_f = \exp(-(V-444)/220), \quad \tau_b = 50$$

with parameter values $C = 5.7$ pF, $I_{app} = 0$ pA, $g_{Na} = 229$ nS, $g_K = 14$ nS, $g_{Ca} = 65$ nS, $g_{BK} = 10$ nS, $g_{Cl} = 0.3$ nS, $g_{K\text{-}leak} = 0.04$ nS, $E_{Na} = 45$ mV, $E_K = -97$ mV, $E_{Ca} = 64$ mV, $E_{Cl} = -60$ mV, and $E_{NALCN} = -20$ mV.

Our SCN model extends previously published versions (Diekman and Forger, 2009; Sim and Forger, 2007) by separating the leak current into sodium, potassium, and chloride components (with parameter values chosen based on our measurements of sodium leak current density and RMP) and by incorporating a large-conductance calcium-activated potassium (BK) current. BK channels are voltage and calcium gated. However, since the nanodomain calcium concentration sensed by the channel reaches equilibrium very quickly, we follow (Tomaiuolo et al., 2012) and model the gating as a purely voltage-dependent process. The differential equations were solved using the Euler-Maruyama method, with a time step of 0.01 ms and standard Gaussian-distributed voltage noise ($\mu = 0$, $\sigma = 0.5$).

SUPPLEMENTAL INFORMATION

Supplemental Information includes Supplemental Experimental Procedures, seven figures, and four tables and can be found with this article online at http://dx.doi.org/10.1016/j.cell.2015.07.036.

AUTHOR CONTRIBUTIONS

R.A., I.M.R., and M.F. designed the experiments; M.F. performed experiments and analyses related to Figures 1, 2, 3, 4, 6C–6H, 7A–7G, S1, S2, S5C, and S6 and Tables S1 and S2; E.K.-E. designed, performed, and analyzed experiments related to Figures 5, 6A, 6B, S3, S5A, and S5D and Tables S3 and S4; A.L.H., K.P.W., and A.R.D. performed RNA-seq analyses related to Figure 5A; C.O.D. developed the mathematical model related to Figures 7H–7J and S7; T.H.H. performed electrophysiological recordings and analyses on lLNvs neurons related to Figure S4; D.L.M. and B.C.L. performed experiments and analyses related to Figure S5B; K.A. and D.R. generated the *NALCN*$^{fx/fx}$ mice; M.F. and R.A. wrote the manuscript; C.O.D. wrote sections related to the mathematical model. I.M.R. edited the manuscript.

ACKNOWLEDGMENTS

We thank B. White and H-S. Li for communicating results prior to publication; M. Vitaterna, K. Shimomura, A. Para, E. Zaharieva, D. Wokosin, C. Olker, and Jordan I. Robson for technical assistance; J. Gu, R. Scott, and B. White for the cloning and generation of UAS-NA^{HA} flies; Dr. Jean Richa (Transgenic and Chimera Mouse Facility at the University of Pennsylvania) for ES cell injection; and M. Gallio for reagents and comments on a draft of the manuscript. We also thank Bloomington *Drosophila* stock center, the National Institute of Genetics (NIG), Vienna *Drosophila* RNAi center (VDRC) for reagents, and the TRiP at Harvard Medical School (NIH/NIGMS R01-GM084947) for providing transgenic RNAi fly stocks. This work was supported by National Institutes of Health (NIH) grants R01NS052903 and R01MH092273 (to R.A.), NS055293 and NS074257 (to D.R.), R00GM080107 (to B.C.L.), and National Science Foundation (NSF) Division of Mathematical Science grant (DMS1412877 to C.O.D.). This effort was in part sponsored by the Defense Advanced Research Projects Agency (DARPA) (D12AP00023, to R.A.); the content of the information does not necessarily reflect the position or the policy of the government, and no official endorsement should be inferred. This work was also supported by the Northwestern University Flow Cytometry Facility, by a Cancer Center Support Grant (NCI CA060553).The two-photon microscope was supported by NINDS (NS054850). A.L.H. is a trainee of the NIH Medical Scientist Training program at the University of Chicago (NIGMS T32GM07281). This work made use of the Open Science Data Cloud (OSDC), which is an Open Cloud Consortium (OCC)-sponsored project. This work was supported, in part, by grants from Gordon and Betty Moore Foundation, the NSF, and major contributions from OCC members like the University of Chicago. Our work is in memory of Howard Nash, who rediscovered *narrow abdomen* and inspired our pursuit of studies of this channel.

Received: December 11, 2014
Revised: May 17, 2015
Accepted: July 6, 2015
Published: August 13, 2015

REFERENCES

Abruzzi, K.C., Rodriguez, J., Menet, J.S., Desrochers, J., Zadina, A., Luo, W., Tkachev, S., and Rosbash, M. (2011). Drosophila CLOCK target gene characterization: implications for circadian tissue-specific gene expression. Genes Dev. *25*, 2374–2386.

Allada, R., and Chung, B.Y. (2010). Circadian organization of behavior and physiology in Drosophila. Annu. Rev. Physiol. *72*, 605–624.

Cao, G., and Nitabach, M.N. (2008). Circadian control of membrane excitability in Drosophila melanogaster lateral ventral clock neurons. J. Neurosci. *28*, 6493–6501.

Casanova, E., Fehsenfeld, S., Mantamadiotis, T., Lemberger, T., Greiner, E., Stewart, A.F., and Schütz, G. (2001). A CamKIIalpha iCre BAC allows brain-specific gene inactivation. Genesis *31*, 37–42.

Cavanaugh, D.J., Geratowski, J.D., Wooltorton, J.R., Spaethling, J.M., Hector, C.E., Zheng, X., Johnson, E.C., Eberwine, J.H., and Sehgal, A. (2014). Identification of a circadian output circuit for rest:activity rhythms in Drosophila. Cell *157*, 689–701.

Colwell, C.S. (2011). Linking neural activity and molecular oscillations in the SCN. Nat. Rev. Neurosci. *12*, 553–569.

de Jeu, M., Hermes, M., and Pennartz, C. (1998). Circadian modulation of membrane properties in slices of rat suprachiasmatic nucleus. Neuroreport *9*, 3725–3729.

Diekman, C.O., and Forger, D.B. (2009). Clustering predicted by an electrophysiological model of the suprachiasmatic nucleus. J. Biol. Rhythms *24*, 322–333.

Diekman, C.O., Belle, M.D., Irwin, R.P., Allen, C.N., Piggins, H.D., and Forger, D.B. (2013). Causes and consequences of hyperexcitation in central clock neurons. PLoS Comput. Biol. *9*, e1003196.

Flourakis, M., and Allada, R. (2015). Patch-clamp electrophysiology in Drosophila circadian pacemaker neurons. Methods Enzymol. *552*, 23–44.

Fogle, K.J., Parson, K.G., Dahm, N.A., and Holmes, T.C. (2011). CRYPTOCHROME is a blue-light sensor that regulates neuronal firing rate. Science *331*, 1409–1413.

Fogle, K.J., Baik, L.S., Houl, J.H., Tran, T.T., Roberts, L., Dahm, N.A., Cao, Y., Zhou, M., and Holmes, T.C. (2015). CRYPTOCHROME-mediated phototransduction by modulation of the potassium ion channel β-subunit redox sensor. Proc. Natl. Acad. Sci. USA *112*, 2245–2250.

Ghezzi, A., Liebeskind, B.J., Thompson, A., Atkinson, N.S., and Zakon, H.H. (2014). Ancient association between cation leak channels and Mid1 proteins is conserved in fungi and animals. Front. Mol. Neurosci. *7*, 15.

Guo, F., Cerullo, I., Chen, X., and Rosbash, M. (2014). PDF neuron firing phase-shifts key circadian activity neurons in Drosophila. eLife *3*, 3.

Hardin, P.E. (2011). Molecular genetic analysis of circadian timekeeping in Drosophila. Adv. Genet. *74*, 141–173.

Helfrich-Förster, C. (2005). Neurobiology of the fruit fly's circadian clock. Genes Brain Behav. *4*, 65–76.

Hughes, M.E., Hogenesch, J.B., and Kornacker, K. (2010). JTK_CYCLE: an efficient nonparametric algorithm for detecting rhythmic components in genome-scale data sets. J. Biol. Rhythms *25*, 372–380.

Humphrey, J.A., Hamming, K.S., Thacker, C.M., Scott, R.L., Sedensky, M.M., Snutch, T.P., Morgan, P.G., and Nash, H.A. (2007). A putative cation channel and its novel regulator: cross-species conservation of effects on general anesthesia. Curr. Biol. *17*, 624–629.

Hutchison, A.L., Maienschein-Cline, M., Chiang, A.H., Tabei, S.M., Gudjonson, H., Bahroos, N., Allada, R., and Dinner, A.R. (2015). Improved statistical methods enable greater sensitivity in rhythm detection for genome-wide data. PLoS Comput. Biol. *11*, e1004094.

Itri, J.N., Michel, S., Vansteensel, M.J., Meijer, J.H., and Colwell, C.S. (2005). Fast delayed rectifier potassium current is required for circadian neural activity. Nat. Neurosci. *8*, 650–656.

Izumo, M., Pejchal, M., Schook, A.C., Lange, R.P., Walisser, J.A., Sato, T.R., Wang, X., Bradfield, C.A., and Takahashi, J.S. (2014). Differential effects of light and feeding on circadian organization of peripheral clocks in a forebrain Bmal1 mutant. eLife *3*, 3.

Jackson, A.C., Yao, G.L., and Bean, B.P. (2004). Mechanism of spontaneous firing in dorsomedial suprachiasmatic nucleus neurons. J. Neurosci. *24*, 7985–7998.

Joiner, W.J., Friedman, E.B., Hung, H.T., Koh, K., Sowcik, M., Sehgal, A., and Kelz, M.B. (2013). Genetic and anatomical basis of the barrier separating wakefulness and anesthetic-induced unresponsiveness. PLoS Genet. *9*, e1003605.

Kaneko, M., Park, J.H., Cheng, Y., Hardin, P.E., and Hall, J.C. (2000). Disruption of synaptic transmission or clock-gene-product oscillations in circadian pacemaker cells of Drosophila cause abnormal behavioral rhythms. J. Neurobiol. *43*, 207–233.

Kudo, T., Loh, D.H., Kuljis, D., Constance, C., and Colwell, C.S. (2011). Fast delayed rectifier potassium current: critical for input and output of the circadian system. J. Neurosci. *31*, 2746–2755.

Kuhlman, S.J., and McMahon, D.G. (2004). Rhythmic regulation of membrane potential and potassium current persists in SCN neurons in the absence of environmental input. Eur. J. Neurosci. *20*, 1113–1117.

Kuhlman, S.J., and McMahon, D.G. (2006). Encoding the ins and outs of circadian pacemaking. J. Biol. Rhythms *21*, 470–481.

Kula-Eversole, E., Nagoshi, E., Shang, Y., Rodriguez, J., Allada, R., and Rosbash, M. (2010). Surprising gene expression patterns within and between PDF-containing circadian neurons in Drosophila. Proc. Natl. Acad. Sci. USA *107*, 13497–13502.

Kunst, M., Hughes, M.E., Raccuglia, D., Felix, M., Li, M., Barnett, G., Duah, J., and Nitabach, M.N. (2014). Calcitonin gene-related peptide neurons mediate sleep-specific circadian output in Drosophila. Curr. Biol. *24*, 2652–2664.

Langmead, B., Trapnell, C., Pop, M., and Salzberg, S.L. (2009). Ultrafast and memory-efficient alignment of short DNA sequences to the human genome. Genome Biol. *10*, R25.

Lear, B.C., Lin, J.M., Keath, J.R., McGill, J.J., Raman, I.M., and Allada, R. (2005). The ion channel narrow abdomen is critical for neural output of the Drosophila circadian pacemaker. Neuron *48*, 965–976.

Lear, B.C., Darrah, E.J., Aldrich, B.T., Gebre, S., Scott, R.L., Nash, H.A., and Allada, R. (2013). UNC79 and UNC80, putative auxiliary subunits of the NARROW ABDOMEN ion channel, are indispensable for robust circadian locomotor rhythms in Drosophila. PLoS ONE *8*, e78147.

Lee, C., Bae, K., and Edery, I. (1998). The Drosophila CLOCK protein undergoes daily rhythms in abundance, phosphorylation, and interactions with the PER-TIM complex. Neuron *21*, 857–867.

Lu, B., Su, Y., Das, S., Liu, J., Xia, J., and Ren, D. (2007). The neuronal channel NALCN contributes resting sodium permeability and is required for normal respiratory rhythm. Cell *129*, 371–383.

Lu, B., Su, Y., Das, S., Wang, H., Wang, Y., Liu, J., and Ren, D. (2009). Peptide neurotransmitters activate a cation channel complex of NALCN and UNC-80. Nature *457*, 741–744.

Meredith, A.L., Wiler, S.W., Miller, B.H., Takahashi, J.S., Fodor, A.A., Ruby, N.F., and Aldrich, R.W. (2006). BK calcium-activated potassium channels regulate circadian behavioral rhythms and pacemaker output. Nat. Neurosci. *9*, 1041–1049.

Michel, S., Geusz, M.E., Zaritsky, J.J., and Block, G.D. (1993). Circadian rhythm in membrane conductance expressed in isolated neurons. Science *259*, 239–241.

Michel, S., Manivannan, K., Zaritsky, J.J., and Block, G.D. (1999). A delayed rectifier current is modulated by the circadian pacemaker in Bulla. J. Biol. Rhythms *14*, 141–150.

Mohawk, J.A., and Takahashi, J.S. (2011). Cell autonomy and synchrony of suprachiasmatic nucleus circadian oscillators. Trends Neurosci. *34*, 349–358.

Nagoshi, E., Sugino, K., Kula, E., Okazaki, E., Tachibana, T., Nelson, S., and Rosbash, M. (2010). Dissecting differential gene expression within the circadian neuronal circuit of Drosophila. Nat. Neurosci. *13*, 60–68.

Nahm, S.S., Farnell, Y.Z., Griffith, W., and Earnest, D.J. (2005). Circadian regulation and function of voltage-dependent calcium channels in the suprachiasmatic nucleus. J. Neurosci. *25*, 9304–9308.

Nash, H.A., Scott, R.L., Lear, B.C., and Allada, R. (2002). An unusual cation channel mediates photic control of locomotion in Drosophila. Curr. Biol. *12*, 2152–2158.

Park, D., and Griffith, L.C. (2006). Electrophysiological and anatomical characterization of PDF-positive clock neurons in the intact adult Drosophila brain. J. Neurophysiol. *95*, 3955–3960.

Park, J.H., Helfrich-Förster, C., Lee, G., Liu, L., Rosbash, M., and Hall, J.C. (2000). Differential regulation of circadian pacemaker output by separate clock genes in Drosophila. Proc. Natl. Acad. Sci. USA *97*, 3608–3613.

Peng, Y., Stoleru, D., Levine, J.D., Hall, J.C., and Rosbash, M. (2003). Drosophila free-running rhythms require intercellular communication. PLoS Biol. *1*, E13.

Pennartz, C.M., de Jeu, M.T., Bos, N.P., Schaap, J., and Geurtsen, A.M. (2002). Diurnal modulation of pacemaker potentials and calcium current in the mammalian circadian clock. Nature *416*, 286–290.

Pitts, G.R., Ohta, H., and McMahon, D.G. (2006). Daily rhythmicity of large-conductance Ca2+ -activated K+ currents in suprachiasmatic nucleus neurons. Brain Res. *1071*, 54–62.

Raman, I.M., Gustafson, A.E., and Padgett, D. (2000). Ionic currents and spontaneous firing in neurons isolated from the cerebellar nuclei. J. Neurosci. *20*, 9004–9016.

Roberts, A., Trapnell, C., Donaghey, J., Rinn, J.L., and Pachter, L. (2011). Improving RNA-Seq expression estimates by correcting for fragment bias. Genome Biol. *12*, R22.

Schaap, J., Pennartz, C.M., and Meijer, J.H. (2003). Electrophysiology of the circadian pacemaker in mammals. Chronobiol. Int. *20*, 171–188.

Seluzicki, A., Flourakis, M., Kula-Eversole, E., Zhang, L., Kilman, V., and Allada, R. (2014). Dual PDF signaling pathways reset clocks via TIMELESS and acutely excite target neurons to control circadian behavior. PLoS Biol. *12*, e1001810.

Shafer, O.T., Rosbash, M., and Truman, J.W. (2002). Sequential nuclear accumulation of the clock proteins period and timeless in the pacemaker neurons of Drosophila melanogaster. J. Neurosci. *22*, 5946–5954.

Sheeba, V., Gu, H., Sharma, V.K., O'Dowd, D.K., and Holmes, T.C. (2008). Circadian- and light-dependent regulation of resting membrane potential and spontaneous action potential firing of Drosophila circadian pacemaker neurons. J. Neurophysiol. *99*, 976–988.

Sim, C.K., and Forger, D.B. (2007). Modeling the electrophysiology of suprachiasmatic nucleus neurons. J. Biol. Rhythms *22*, 445–453.

Swayne, L.A., Mezghrani, A., Varrault, A., Chemin, J., Bertrand, G., Dalle, S., Bourinet, E., Lory, P., Miller, R.J., Nargeot, J., and Monteil, A. (2009). The NALCN ion channel is activated by M3 muscarinic receptors in a pancreatic beta-cell line. EMBO Rep. *10*, 873–880.

Tomaiuolo, M., Bertram, R., Leng, G., and Tabak, J. (2012). Models of electrical activity: calibration and prediction testing on the same cell. Biophys. J. *103*, 2021–2032.

Xie, L., Gao, S., Alcaire, S.M., Aoyagi, K., Wang, Y., Griffin, J.K., Stagljar, I., Nagamatsu, S., and Zhen, M. (2013). NLF-1 delivers a sodium leak channel to regulate neuronal excitability and modulate rhythmic locomotion. Neuron *77*, 1069–1082.

Yang, Z., and Sehgal, A. (2001). Role of molecular oscillations in generating behavioral rhythms in Drosophila. Neuron *29*, 453–467.

Yao, Z., and Shafer, O.T. (2014). The Drosophila circadian clock is a variably coupled network of multiple peptidergic units. Science *343*, 1516–1520.

Zhang, L., Chung, B.Y., Lear, B.C., Kilman, V.L., Liu, Y., Mahesh, G., Meissner, R.A., Hardin, P.E., and Allada, R. (2010a). DN1(p) circadian neurons coordinate acute light and PDF inputs to produce robust daily behavior in Drosophila. Curr. Biol. *20*, 591–599.

Zhang, Y., Liu, Y., Bilodeau-Wentworth, D., Hardin, P.E., and Emery, P. (2010b). Light and temperature control the contribution of specific DN1 neurons to Drosophila circadian behavior. Curr. Biol. *20*, 600–605.

Cell

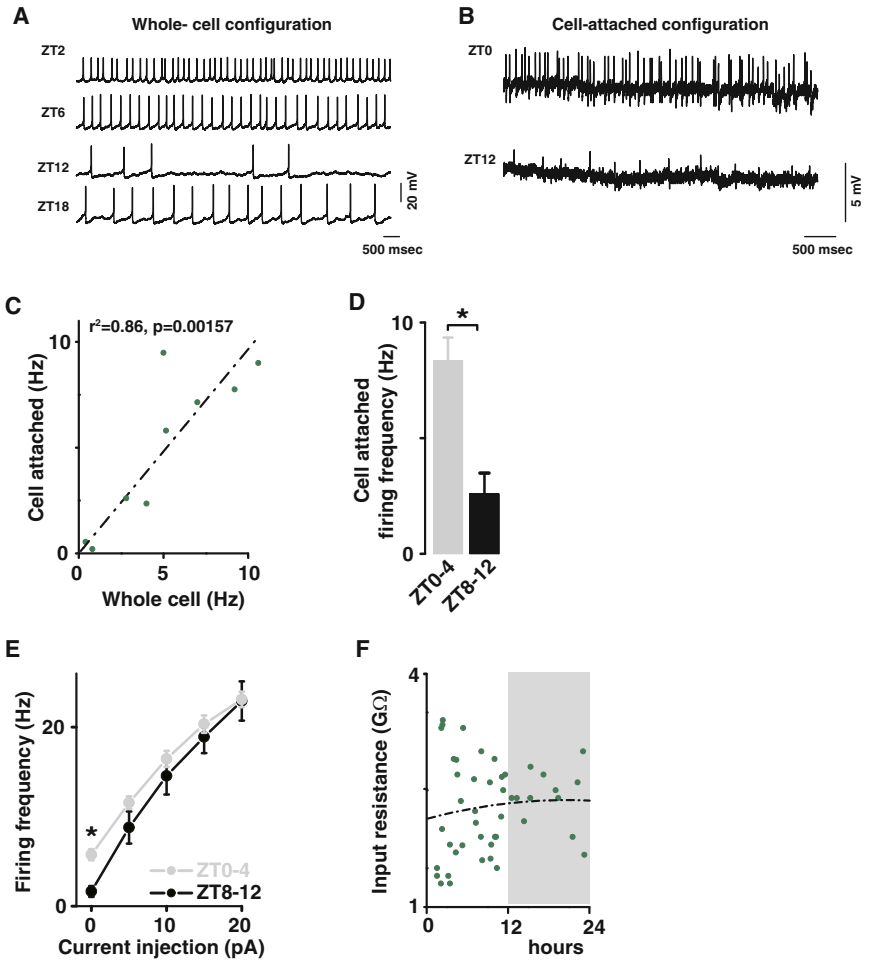

Figure S1. Patch-Clamp Analysis of DN1p Neurons Demonstrates Robust Rhythms of Membrane Excitability, Related to Figure 1

(A) Four representative whole-cell current-clamp recordings from four different DN1ps obtained at different times of day (from top to bottom: ZT2, 6, 12, 18) and (B) two representative cell-attached current-clamp recordings from 2 different DN1ps obtained at ZT0 and 12 show rhythms in firing frequency. (C) Recording from same cells in both cell-attached mode and whole-cell mode shows similar firing frequency (linear regression: $r^2 = 0.86$, $p = 0.00157$, $n = 9$). (D) Cell-attached recordings confirm rhythms of firing frequency (8.3 ± 1 Hz, n = 5 at ZT0-4 and 2.6 ± 0.9 Hz, n = 5 at ZT8-12, p = 0.003). (E) In whole-cell configuration, depolarizing current injections in wild-type also shows rhythms in cellular excitability. f-I curves of *WT* measured at ZT0-4 versus ZT8-12 ($p < 0.001$) (respectively gray and black). (F) All recorded *WT* neurons (green dots) are plotted against time of day for input resistance. Results are expressed as mean ± SEM.

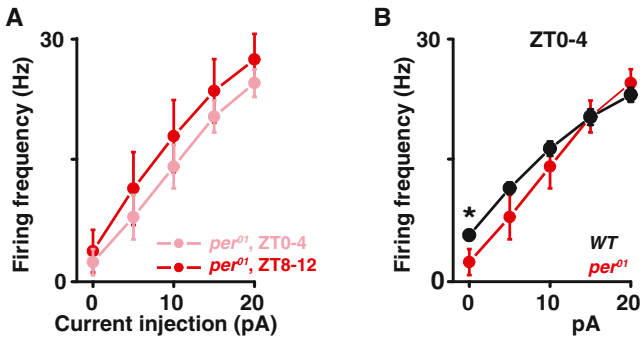

Figure S2. The Rhythmic Membrane Properties of the *Drosophila* Circadian Pacemaker Neurons Are Clock Controlled, Related to Figure 1

Depolarizing current injections confirms the lack of rhythms in cellular excitability in the per^{01} neurons (light red: ZT0, dark red ZT12, $p > 0.41$) (A) and the decrease in cellular excitability in the per^{01} neurons (red) versus wild-type (black) (B). Results are expressed as mean ± SEM. Asterisks indicate statistical significance (t test, $p < 0.05$).

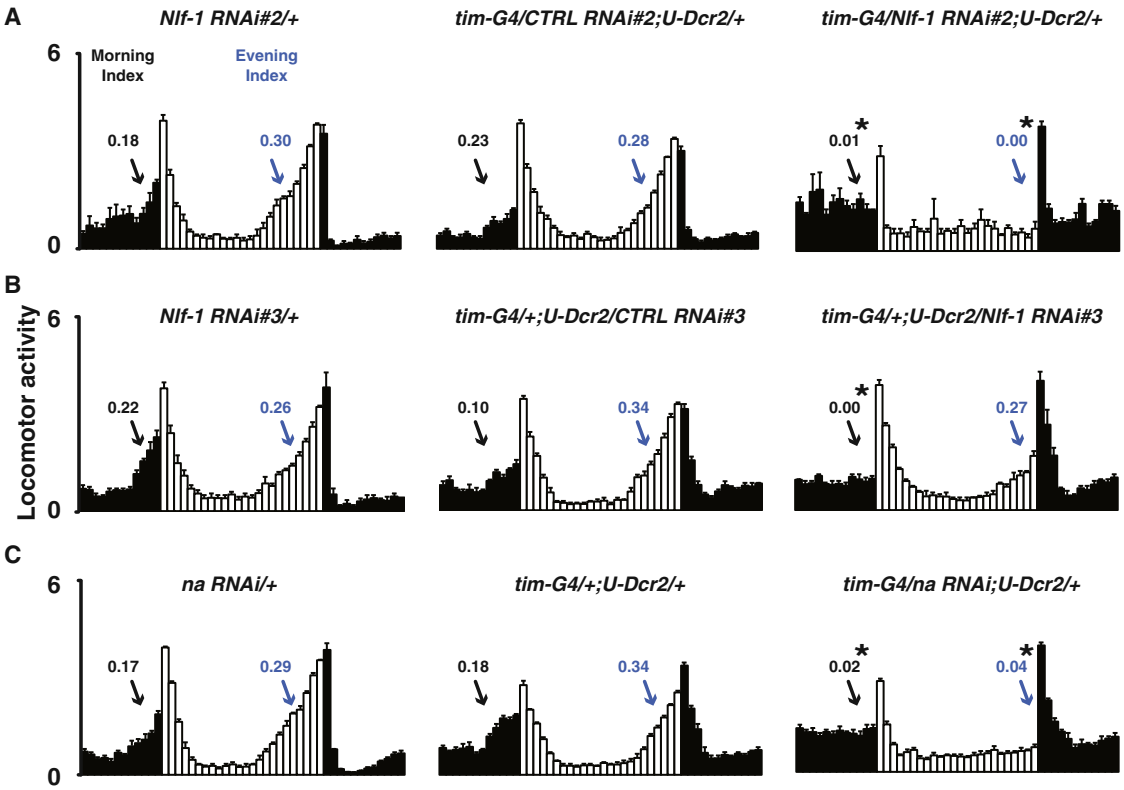

Figure S3. *Nlf-1* Expression Is Required for Diurnal Rhythmic Activity, Related to Figure 6

(A) *Nlf-1* RNAi #2 (from VDRC), (B) *Nlf-1* RNAi #3 (from NIG, Japan), (C) *na* RNAi (from VDRC) lines were crossed to the broad circadian driver tim-G4. The *Nlf-1* or *na* knockdown flies (tim-G4/*Nlf-1* RNAi #2;U-Dcr2/+ in (A), tim-G4/+;U-Dcr2/*Nlf-1* RNAi #3 in (B) and tim-G4/*na* RNAi;U-Dcr2/+ in (C) were compared to their appropriate genetic controls (respectively *Nlf-1* RNAi#2/+ and tim-G4/*CTRL* RNAi #2;U-Dcr2/+ in (A), *Nlf-1* RNAi #3/+ and tim-G4/+;U-Dcr2/ *CTRL* RNAi #3 in (B), *na* RNAi/+ and tim-G4/+;U-Dcr2/+ in (C). Morning Index (black) and Evening Index (blue) are measures of morning/evening anticipation, respectively. Asterisks indicate differences statistically significant in comparison to controls (ANOVA, $p < 0.02$).

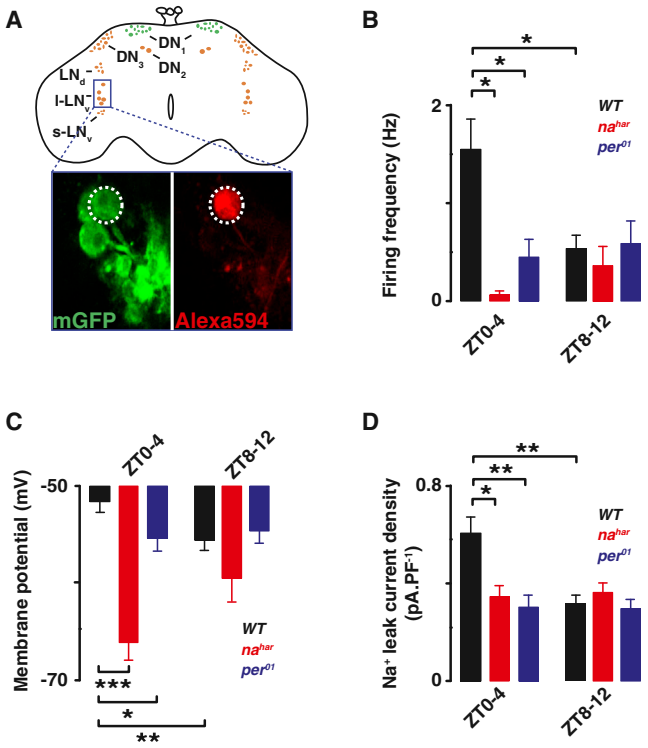

Figure S4. The Cellular Excitability and NA Current of the *Drosophila* l-LNvs Circadian Pacemaker Neurons Are Clock Controlled, Related to Figure 6

(A) Schematic and image of the *Drosophila* brain indicating the location of the l-LNvs and other clock neurons. Representative images of the GFP-expressing l-LNvs in the intact *Drosophila* brain are shown below. The l-LNvs were labeled by using the Pdf-G4 driving the expression of U-CD8-GFP. Whole-cell access to GFP labeled neurons was confirmed following diffusion of Alexa Fluor 594 biocytin included in intracellular recording solution. Histograms showing rhythms in wild-type (*WT*) and the decrease and lack of rhythms in firing frequency (B), membrane potential (C) and sodium leak current density (D) in na^{har} (red) and per^{01} (blue) when compared to *WT* (black) l-LNvs neurons (respectively for *WT*: 1.5 ± 0.3Hz, −57 ± 1.1mV, 0.6 ± 0.1pA.pF^{-1} n = 18 at ZT0-4 and 0.7 ± 0.2Hz, -55.6 ± 1.1mV, 0.3 ± 0.0pA.pF^{-1}, n = 13 at ZT8-12; for na^{har}: 0.1 ± 0.0Hz, −66.2 ± 2.0mV, 0.3 ± 0.0pA.pF^{-1} n = 11 at ZT0-4 and 0.4 ± 0.2Hz, -59.5 ± 2.4mV, 0.4 ± 0.0pA.pF^{-1}, n = 11 at ZT8-12; for per^{01}: 0.4 ± 0.2Hz, −55.4 ± 1.3mV, 0.3 ± 0.0pA.pF^{-1} n = 11 at ZT0-4 and 0.6 ± 0.2Hz, -55.2 ± 1.2mV, 0.30 ± 0.0pA.pF^{-1}, n = 12 at ZT8-12). Results are expressed as mean ± SEM. Asterisks indicate statistical significance ($p < 0.05$) from t test.

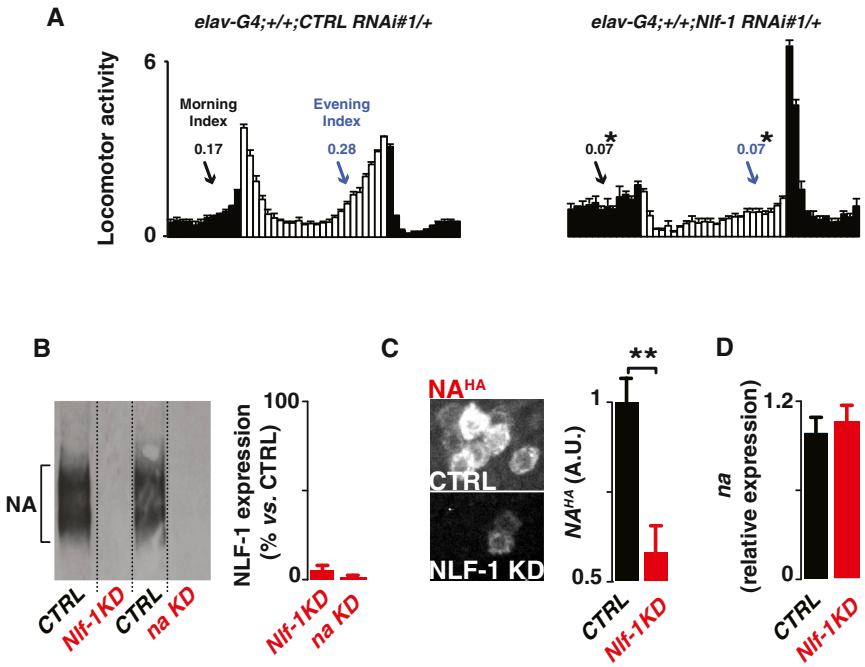

Figure S5. *Nlf-1* Expression Is Required for NA Expression, Related to Figure 6

(A) Morning and evening anticipation are reduced in *Nlf-1* knockdown flies (*CTRL*: *elav-G4;; CTRL RNAi#1/+ versus Nlf-1* RNAi expressing flies (*Nlf-1 KD: elav-G4;; Nlf-1 RNAi#1/+)*. (B) Western blot analyses show reduction in NA expression in *Nlf-1* RNAi expressing flies (*Nlf-1 KD: elav-G4;; Nlf-1 RNAi#1)* (2 left lanes) versus control flies (*CTRL*: *elav-G4;; CTRL RNAi#1/+)* and *na* RNAi expressing flies (*na KD: elav-G4; na RNAi:U-Dcr2/+)* (2 right lanes) versus control flies (*CTRL*: *elav-G4; CTRL RNAi#2/+)*. Quantitation of total levels is shown (n = 2). (C) Anti-HA immunostaining of DN1ps in *CTRL* (top: U-CD8-GFP/U-na^{HA}; Clk4.1M-G4/+) and in *Nlf-1* RNAi expressing flies (bottom: U-CD8-GFP/U-na^{HA}; Clk4.1M-G4/ *Nlf-1 RNAi#1)*. Quantification of total NA^{HA} levels is shown (p = 0.0032). From FACS sorted DN1p neurons, *na* mRNA levels were indistinguishable in *Nlf-1* RNAi expressing flies U-CD8-GFP/+; Clk4.1M-G4/ *Nlf-1 RNAi#1) versus* controls (U-CD8-GFP/+; Clk4.1M-G4/ *CTRL RNAi#1,* n = 2*)* (D). Results are expressed as mean ± SEM.

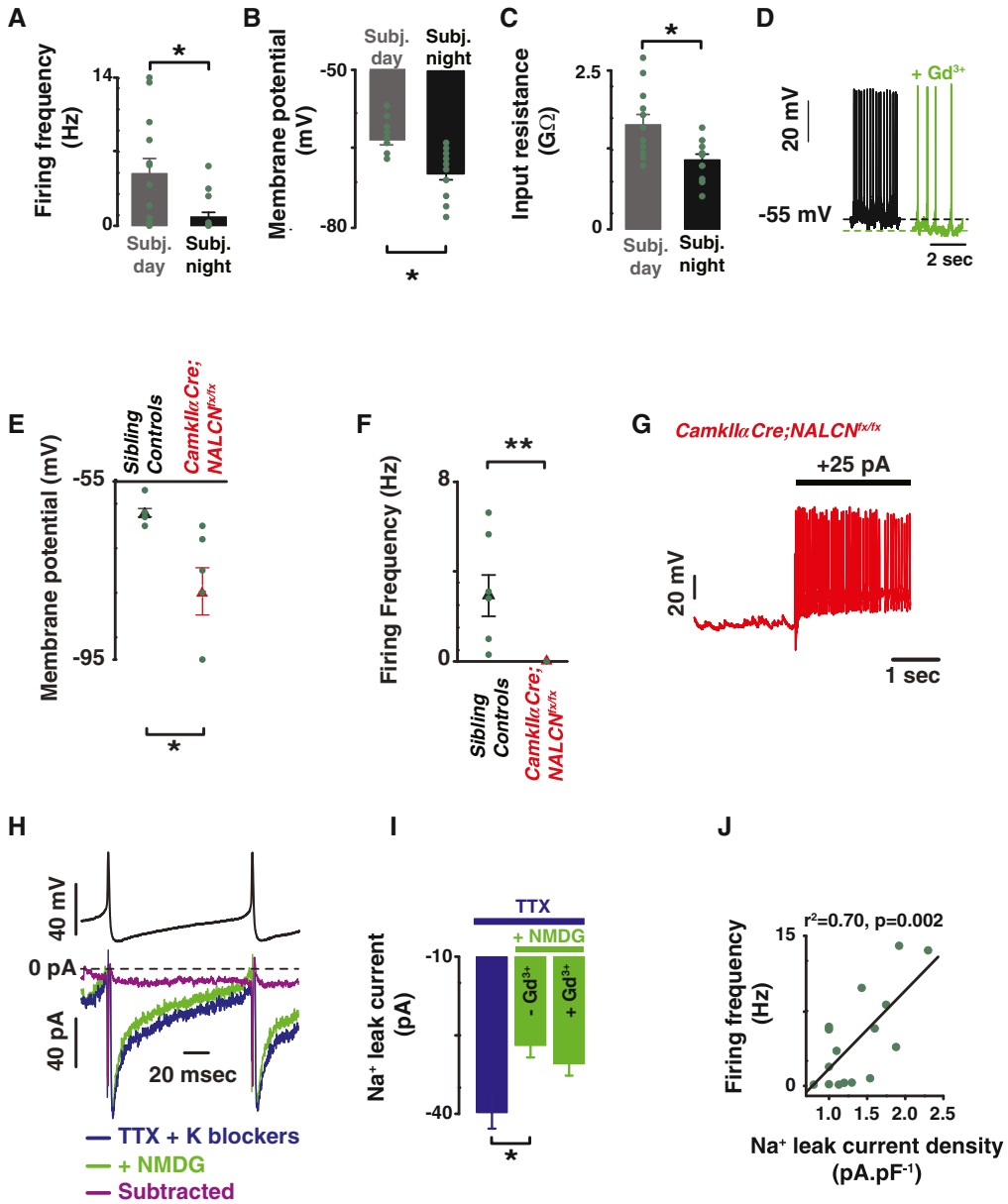

Figure S6. Rhythmic Membrane Properties of Wild-Type and NALCN Knockout SCN Pacemaker Neurons, Related to Figure 7

Circadian variations of firing frequency (A), membrane potential (B) and input resistance (C) were detected (during the subjective day: 4.9 ± 1.4 Hz, −63 ± 0.9mV, 1.6 ± 0.1GΩ (n = 16), and during the subjective night: 0.8 ± 0.4Hz, −69.3 ± 1.1mV, 1.1 ± 0.1GΩ (n = 11), respectively). Green dots represent individual cells. The sodium leak observed in the SCN neurons shares identical properties to NALCN: blocking the sodium leak with Gd^{3+} hyperpolarizes the neurons and decreases firing rate (D). Membrane potential (E) and firing frequency (F) of *CamkIIa-Cre;NALCN$^{fx/fx}$* (red triangle) versus sibling controls (black triangle) (0Hz, −81.2 ± 5.3mV in *CamkIIa-Cre;NALCN$^{fx/fx}$*, (n = 6) and 2.9 ± 0.9Hz, −63.5 ± 0.9mV in sibling controls (n = 7), respectively). (G) High firing frequency can be restored in *CamkIIa-Cre;NALCN$^{fx/fx}$* neurons by injecting a depolarizing current (+25pA). (H) Action potential clamp recordings showing the sodium leak flowing during the interspike interval in SCN neurons. Top panel shows recorded action potentials used as a voltage command to measure currents flowing during the interspike interval (bottom panel). Blue trace represent currents recorded in the presence of TTX and K blockers. The sodium leak current flowing during the interspike interval was revealed after sodium substitution with NMDG (green trace). Subtracted currents (purple trace) were calculated by subtracting the currents recorded with NMDG to the currents recorded without NMDG. The pharmacological profile of this sodium leak is shown in (I) (TTX-resistant in blue, NMDG and Gd^{3+} sensitive (in green). Asterisks indicate statistical significance (t test, $p < 0.05$). (J) During the subjective day, I_{NALCN} is positively correlated to firing frequency and (linear regression: $r^2 = 0.68$, $p = 0.019$); individual cells are shown in green dots. Results are expressed as mean ± SEM.

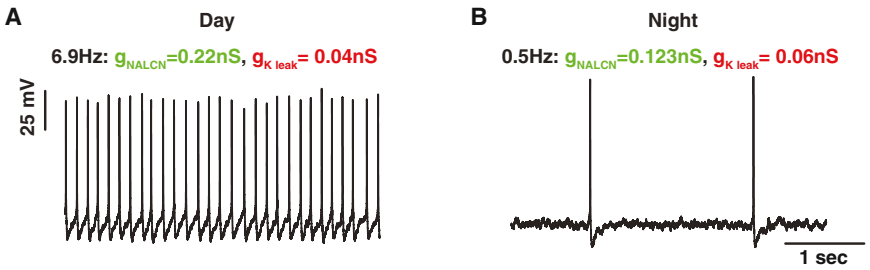

Figure S7. Modulation of Sodium and Potassium Leak Conductances in a Mathematical Model of SCN Membrane Excitability, Related to Figure 7

Voltage traces from our simulations are shown with (A) $g_{K\text{-}leak}$ = 0.04 and g_{NALCN} = 0.22 nS, and (B) $g_{K\text{-}leak}$ = 0.06 and g_{NALCN} = 0.123 nS.

Cell

Supplemental Information

A Conserved Bicycle Model for Circadian Clock Control of Membrane Excitability

Matthieu Flourakis, Elzbieta Kula-Eversole, Alan L. Hutchison, Tae Hee Han, Kimberly Aranda, Devon L. Moose, Kevin P. White, Aaron R. Dinner, Bridget C. Lear, Dejian Ren, Casey O. Diekman, Indira M. Raman, and Ravi Allada

Supplemental Experimental Procedures

Electrophysiological recordings from *Drosophila* circadian neurons

Whole brain electrophysiology experiments were performed on an Ultima two-photon laser scanning microscope (Bruker, former Prairie Technologies, Middleton, WI) equipped with galvanometers driving a Coherent Chameleon laser. Fluorescence was detected with photomultiplier tube. Images were acquired with an upright Zeiss Axiovert microscope with a 40×0.9 numerical aperture water immersion objective at 512 pixels × 512 pixels resolution and 1-μm steps. Current-clamp and voltage-clamp recordings were performed with pipettes (10–14 MΩ) filled with internal solution containing the following (in mM): 102 K-gluconate, 0.085 $CaCl_2$ 1.7, $MgCl_2$, 17 NaCl, 0.94 EGTA, 8.5 HEPES, 4 Mg-ATP, 0.3 Tris-GTP, and 14 phosphocreatine (di-tris salt), pH 7.2, 235 Osm. To visualize the recorded cell, Alexa Fluor 594 biocytin (10μM) was added into the intracellular solution. Recordings were made using Axopatch 200B patch-clamp amplifier, digitized with a Digidata 1320 A, and acquired with pCLAMP software (Axon Instruments, Union City, CA). The sodium leak current (I_{Na}) was examined in the presence of TTX (10μM), TEA (10mM), 4-AP (5mM) and CsCl (2mM), and I_{Na} was revealed by replacing the extracellular sodium with NMDG (Lu et al., 2007). In voltage-clamp mode, a step protocol (from -113mV to +87mV steps for 300ms) was used to study inward currents. All recordings were corrected for liquid junction potential (13mV). Most chemicals were purchased from Sigma (St Louis, MO). For analysis, cells with high series resistance or with low membrane resistance (<1GΩ) were discarded.

Electrophysiological recordings from SCN neurons

For patch-clamp experiments, slices were transferred to an incubating chamber and continuously

perfused with oxygenated ACSF throughout the recording period. Slices were kept at 35°C for at least 20 min and no more than 3 h before recording. Current-clamp and voltage-clamp recordings were performed with pipettes (5–8 MΩ) filled with internal solution containing the following in mM: 130 K-gluconate, 2 $MgCl_2$, 10 KCl, 0.5 EGTA, 20 HEPES, 4 Mg-ATP, 0.3 Tris-GTP, and 14 phosphocreatine (di-tris salt), pH 7.3, 280-290 mOsm. To avoid loss of critical intracellular components after break-in, membrane properties were obtained in the initial 4 minutes of being in the whole-cell configuration. The firing frequency was measured during a 1-minute recording. The input resistance was measured by injecting small hyperpolarizing currents from -5pA to -25pA (5pA increment). For spontaneously active neurons, a small hyperpolarizing holding current was injected to silence the cell. The input resistance was calculated by measuring the slope of the obtained VI curve. The action-potential clamp technique was done as described in (Jackson et al., 2004). Action potentials were recorded in "fast" current clamp mode of an AxoPatch200B amplifier to avoid distortion. The recorded action potentials were then used as a command in voltage-clamp mode. The series resistance was compensated to allow accurate current measurements. All recordings were corrected for liquid junction potential (16.5mV). For analysis, cells with high series resistance or with low membrane resistance (<1GΩ) were discarded.

Fluorescence activated cell sorting of DN1p neurons

DN1p neurons were labeled with GFP using the Clk4.1M-G4 driver. Brains were dissected and processed as described previously (Kula-Eversole et al., 2010). Before FACS cell sorting cells were filtered using 100μM filter and propidium iodide (130ng/ul) was added to distinguish between dead and alive cells. Cells were sorted on Aria II FACS Cell Sorter (BD Biosciences)

into an extraction buffer in the Northwestern Flow Cytometry facility. Subsequently, the cells were lysed and stored at -80°C until RNA extraction as described previously (Nagoshi et al., 2010). We typically used 300-500 cells from 40-45 brains per time points for mRNA isolation.

Drosophila genetics and circadian behavioral assay

na^{har}, per^{01} or *wild-type* virgin females were crossed to *U-CD8-GFP; Clk4.1M-G4/TM6C* males flies. Respectively wild type, na^{har}; U-CD8-GFP /+; Clk4.1M-G4/+ or per^{01}; U-CD8-GFP /+; Clk4.1M-G4/+ males were collected from each cross at least 24h before recordings. For rescue experiments, na^{har}*;; U-na virgin* flies were crossed to *U-CD8-GFP; Clk4.1M-G4/TM6C* males and na^{har} *; U-CD8-GFP /+; U-na/Clk4.1M-G4* males were collected for recordings. To generate the *Nlf-1* knockdown flies for electrophysiological recordings, the RNAi line (RNAi#1: BDSC#36754) or the appropriate background control were crossed to *U-CD8-GFP; Clk4.1M-G4/TM6C*. Adult progeny were kept in an entrainment incubator with a 12 hours light: 12 hours dark (LD) cycle at 25C until recording.

For targeted expression of our V5 3' tagged *Nlf-1* construct, the *nlf-1* coding sequence was amplified from a cDNA library (Phusion polymerase, NEB), where the tag was incorporated into the reverse primer. Primer sequences were as following: forward primer: CAAACATGCGGCCAGGACCCGGGCTGGTC, reverse primer: CTACGTGCTATCTAGACCAAGAAGAGGGTTAGGTATAGGCTTACCTAAGGCCCCGCT GCTCAGG. The *Nlf-1* PCR fragment was cloned into a TOPO TA plasmid vector, following the manufacturer's instructions (Invitrogen, kit No. K2520). The final expression construct was obtained using the Gateway system, following the manufacturer's instructions (Invitrogen, kit No. 11791-020). In brief, pCR8/GW/TOPO-$NLF1^{V5}$ was recombined with pGTW (a *Drosophila*

pUAST Gateway vector developed in the laboratory of Dr. Marco Gallio, Northwestern University) to obtain pGTW-NLF1^{V5}. The correct *nlf-1* sequence from pGTW-NLF1 was verified by sequencing. Transgenic flies were obtained by phiC31-mediated transformation using attP2 landing sites (BestGene, Inc). UAS-NA^{HA} was generated by using GalK-mediated recombineering to insert an HA tag in the S5-S6 (I) region: …NNTEYDLYPYDVPDYADLYKR….

For behavioral experiments, transgenic flies carrying RNAi constructs were obtained from the Transgenic RNAi Project (TRiP) (Nlf-1 RNAi#1: BDSC#36754 and control CTRL RNAi#1: #36303), Vienna Drosophila RNAi Center (VDRC) (Nlf-1 RNAi#2: VDRC#v107439, na RNAi: VDRC#v103754 and control CTRL RNAi#2: #60100) and National Institute of Genetics (NIG) (RNA#3: NIG#13595-R3 and control CTRL RNAi#3: NIG w1118). The RNAi lines were used to generate the *Nlf-1 or na* knockdown flies. For behavioral experiments, the RNAi lines or appropriate controls were crossed to *tim-G4;U-Dcr2*. Fly behavior was recorded using the Drosophila Activity Monitoring system (Trikinetics) and analyzed using ClockLab and the Counting Macro as described (Pfeiffenberger et al., 2010). Briefly, male flies were fed on 5% sucrose-agar medium in 5LD7DD conditions at 25C. LD eductions were obtained using averaged data in 30-minute bins across days 2–5 of the behavior run. DD period and rhythmicity data were calculated in ClockLab with period measurements taken only from flies in which the Power-Significance (P-S) ≥10. Morning and evening anticipations (increase in activity before lights on or off) were calculated as follows: activity from each of four days of LD behavior recorded for each individual fly was analyzed such that the morning/evening index = ((total activity 3 h prior to lights-on or off)/(total activity 6 h prior to lights-ON or OFF)) - (0.5). 0.5 was subtracted so flat activity over the six hours analyzed is equal to 0. This is a variant of the

method described in (Harrisingh et al., 2007).

Drosophila brain dissection

The dissection protocol was adapted from Gu and O'Dowd (Gu and O'Dowd, 2007) and detailed in (Flourakis and Allada, 2015). Brains from male adults *Drosophila* were removed from their heads in ice-cold control recording solution (in mM: 101 NaCl, 1 $CaCl_2$, 4 $MgCl_2$, 3 KCl, 5 glucose, 1.25 NaH_2PO_4, and 20.7 $NaHCO_3$, pH 7.2, 250 mOsm). The connective tissue, air sacs, and trachea were removed with fine forceps. No enzymatic treatment was used to avoid removing ion channels from the cell surface. Brains were then transferred to a recording chamber for electrophysiological recordings. Brains were held ventral side down by a harp slice grid with silica fibers from ALA scientific. Brains were allowed to rest in continuously flowing oxygenated saline (95% oxygen and 5% carbon dioxide) for at least 10 min and no more than 2 h before recording. Perfusion with oxygenated saline was continued throughout the recording period. Time of recording is used to determine Zeitgeber Time (ZT).

Mice and brain slice preparation

All animal care and handling procedures were conducted according to IACUC approved methods. 3-month-old C57BL6 *wild-type* mice were housed in light-tight boxes to maintain a 12 hours light: 12 hours dark (LD) or 12 hours dark: 12 hours light (DL) schedule for two weeks. Each animal was housed in a cage that contains a running wheel (10 cm diameter), whereby a switch transmitted a signal for every revolution of the wheel. Following two weeks of acclimation, the mice were either sacrificed for patch-clamp experiments or switched to constant darkness (DD) for at least three weeks to monitor their free running period. For each animal the

onset of activity was calculated using ClockLab (Actimetrics, Wilmette, IL) and each animal was then sacrificed at either Circadian Time (CT2- subjective day) or CT14 (subjective night) depending on experimental time needed. The brain was quickly removed and placed in oxygenated ice-cold low Ca^{2+} Artificial CerebroSpinal Fluid slicing solution (low Ca^{2+} ACSF) (composition in mM: 95 NaCl, 0.5 $CaCl_2$, 7 $MgSO_4$, 1.8 KCl, 15 glucose, 1.2 KH_2PO_4, 26 $NaHCO_3$, and sucrose 50, pH 7.4, 300 mOsm). A vibrating blade microtome was used to obtain a 300μM thick slice containing the paired SCN. The slices were then transferred and incubated for at least 1 hour in regular oxygenated ACSF (composition in mM: 127 NaCl, 2.4 $CaCl_2$, 1.3 $MgSO_4$, 1.8 KCl, 15 glucose, 1.2 KH_2PO_4, and 26 $NaHCO_3$, pH 7.4, 300 mOsm) at room temperature.

Generation of a brain specific knockout of NALCN.

The *NALCN*$^{fx/fx}$ mice were generated using an ES cell line (in the C57BL6 background, from KOMP) with NALCN's exons 4 and 5 floxed. The β-gal and neomycin-resistance genes from the targeting vector were removed by crossing the mice to Flippase mice. Brain specific knockout animals were generated by crossing the *CamkIIa-Cre mice* (Casanova et al., 2001) to the *NALCN*$^{fx/fx}$ mice. Because *CamkIIa-Cre;NALCN*$^{fx/fx}$ animals die at ~21 days, animals were genotyped and sacrificed between P17 and P21 and organotypic slices containing the SCN were obtained as previously described. All animals (males) were age-matched for electrophysiological recordings.

Statistical analysis

Electrophysiological analyses were performed using Clampfit 9 (Axon Instruments, Union City,

CA). Statistical analyses were performed and graphs were generated using Origin (Originlab, Northampton, MA, USA). The results were expressed as mean±S.E.M. Most statistical tests were two sample student t-test and differences were considered statistically significant when $p<0.05$. Where appropriate in the graphs, * denotes $p<0.05$ and ** denotes $p<0.001$. For analyses of daily rhythms in membrane properties and transcripts expression, one-way ANOVA Tukey's post-hoc test was used to compare different time points and genotypes.

mRNA analysis by qPCR in *Drosophila*.

Cells were processed as described previously (Kula-Eversole et al., 2010). cDNA from three independent replicas were analyzed per time-point on a BioRad CFX384 real-time PCR system. mRNA was quantified as described previously (Nagoshi et al., 2010). ANOVA was used to determine statistically significant differences between time-points ($p<0.05$). The following primers were used to examine gene expression:

For *Nlf*-1 knockdown	forward 5'-GACTTGCAGGGTCAGTGCTC-3',
	reverse 5'-CCGCATCTGGGTTGTCTTAT-3'.
Nlf-1 cycling	forward, 5'-CGGACTCCGAAGTGGATAAG-3',
	reverse 5'- ACGACGCTTACGGAACTCTG-3'.
Calmodulin	forward 5'-GGCACCATCACAACAAAGG-3',
	reverse 5'-CTTCTCGGATCTCCTCTTCG-3'.

Western blot.

Western blot experiments and quantitation were performed similarly to previous reports (Lear et al., 2013; Lear et al., 2005). Briefly, adult head extracts were obtained from mixed light phase samples (ZT 0-10), and equal amounts of protein were loaded in each lane as determined by

Bradford assay (BioRad). Lane order was varied between experiments to control for uneven transfer. Blots were probed with Rabbit anti-NA (Nash et al., 2002), and protein levels were measured using NIH ImageJ gel analysis (http://rsbweb.nih.gov/ij/). To account for intensity differences based on exposure, protein levels were normalized to the average intensity of each sample within the blot (Aldridge et al., 2008).

Drosophila brain immunostaining.

Immunostainings were performed as described previously (Seluzicki et al., 2014). Briefly, flies were entrained in 12-h light, 12-h dark (LD) cycles at 25°C. Brains were dissected in PBS (pH 7.5) and fixed in PBS + 3.7% formaldehyde for 1h shaking at room temperature. After three PBT (PBS + 0.3% Triton X-100) rinses, the primary antibody solution (rat anti-HA (1:800)) was added in a solution of PBS, 10% goat normal serum (GNS), and 0.3% Triton X-100. Brains were incubated for three nights shaking at 4°C. After the primary incubation, brains were washed 3× in PBS +0.3% Triton X-100 and secondary antibody (for HA: goat anti-rat Alexa 594, Molecular probes) was added at 1:500. Fluorescence intensity levels were measured using NIH ImageJ.

Table S1. Diurnal Variation of Membrane Properties and I_{NA} in DN1p Neurons, Related to Figures 1, 3, and 6

A: Diurnal Variation of Firing Frequency (in Hz±SEM)

	Wild type		***na*^{har}**	
ZT0-4	8.55±0.78	n=19	0	n=6
ZT4-8	5.50±1.22	n=15	0	n=8
ZT8-12	1.59±0.41	n=23	0	n=8
ZT12-16	0.22±0.22	n=8	0	n=3
ZT16-20	4.20±1.09	n=3	0	n=3
ZT20-24	8.03±1.34	n=4	0	n=3

B: Diurnal Variation of Membrane Potential (in mV±SEM)

	Wild type		***na*^{har}**	
ZT0-4	-49.05±0.67	n=19	-65.33±1.71	n=6
ZT4-8	-51.93±1.59	n=15	-64.12±1.61	n=8
ZT8-12	-57.93±0.99	n=23	-67.44±1.55	n=8
ZT12-16	-59.29±0.97	n=8	-63.00±1.53	n=3
ZT16-20	-54.13±0.47	n=3	-65.00±2.31	n=3
ZT20-24	-49.00±0.41	n=4	-65.00±1.73	n=3

C: Diurnal Variation of Input Resistance (in GΩ±SEM)

	Wild type	
ZT0-4	2.15±0.27	n=11
ZT4-8	2.40±0.16	n=10
ZT8-12	2.22±0.15	n=13
ZT12-16	2.42±0.11	n=5
ZT16-20	2.53±0.09	n=3
ZT20-24	2.50±0.32	n=3

D: Diurnal Variation of I_{NA} (in pA.pF^{-1}±SEM)

	Wild type		**na^{har}**	
ZT0-4	1.91±0.24	n=8	1.23±0.07	n=4
ZT4-8	1.41±0.09	n=5	1.06±0.11	n=5
ZT8-12	1.06±0.12	n=8	1.09±0.06	n=4
ZT12-16	0.61±0.01	n=4	0.86±0.09	n=3
ZT16-20	1.55±0.26	n=4	0.84±0.09	n=3
ZT20-24	1.71±0.04	n=4	0.89±0.16	n=3

Table S2. Depolarizing Current Injections in *WT*, *per*^{01}, *na*^{har}, *na*^{har}*;;U-na/Clk4.1M-G4*, and *Nlf-1 KD,* Related to Figures 1, 3, and 6

A: f-I curves at ZT0-4 vs ZT8-12 in *WT* (in Hz±SEM)

I injected	ZT0-4 (n=8)	ZT8-12 (n=5)
0pA	5.75±0.62	1.64±0.61
5pA	11.56±0.71	8.78±1.79
10pA	16.45±0.89	14.55±2.07
15pA	20.34±0.97	18.90±1.80
20pA	23.10±0.86	22.92±2.19

B: f-I curves at ZT0-4 vs ZT8-12 in *per*^{01} (in Hz±SEM)

I injected	ZT0-4 (n=5)	ZT8-12 (n=4)
0pA	2.42±1.60	3.78±2.63
5pA	7.98±2.75	11.52±4.51
10pA	14.22±2.67	18.00±4.46
15pA	20.42±1.97	23.60±3.91
20pA	24.56±1.71	27.47±3.17

C: f-I curves at ZT0-4 vs ZT8-12 in *na*^{har} (in Hz±SEM)

I injected	ZT0-4 (n=5)	ZT8-12 (n=5)
0pA	0	0
5pA	0.84±0.53	1.22±0.77
10pA	6.06±1.19	4.87±0.51
15pA	11.42±1.47	11.70±1.21
20pA	15.36±1.70	15.65±1.01

D: f-I curves at ZT6 in WT, *na*^{har} and *na*^{har}*;;U-na/Clk4.1M-G4* (in Hz±SEM)

I injected	*WT* (n=10)	*na*^{har} (n=8)	*na*^{har};;U-na/Clk4.1M-G4(n=3)
0pA	3.24±0.86	0	5.95±2.58
5pA	9.99±1.66	2.61±1.23	12.83±2.06
10pA	15.08±1.66	7.82±1.54	17.83±2.72
15pA	19.10±1.48	14.57±2.13	22.20±2.90
20pA	22.57±1.65	20.90±3.32	25.63±3.12

E: f-I curves at ZT0-4 in *Nlf-1 CT* and *Nlf-1 KD* (in Hz±SEM)

I injected	*Nlf-1 CT* (n=3)	*Nlf-1 KD* (n=7)
0pA	1.7±0.93	0
5pA	6.5±2.24	0.13±0.09
10pA	9.53±2.61	3.24±0.86
15pA	12.3±2.90	7.53±1.53
20pA	14.13±3.38	11.03±1.71

F: f-I curves at ZT8-12 in *Nlf-1 CT* and *Nlf-1 OX* (in Hz±SEM)

I injected	*Nlf-1 CT* (n=4)	*Nlf-1 OX* (n=5)
0pA	0	3.18±0.84
5pA	3.62±1.32	10.36±1.17
10pA	9.38±1.87	17.02±1.14
15pA	14.1±2.21	21.76±1.11
20pA	17.34±2.32	24.8±1.17

Supplemental References

Aldridge, G.M., Podrebarac, D.M., Greenough, W.T., and Weiler, I.J. (2008). The use of total protein stains as loading controls: an alternative to high-abundance single-protein controls in semi-quantitative immunoblotting. Journal of neuroscience methods *172*, 250-254.

Casanova, E., Fehsenfeld, S., Mantamadiotis, T., Lemberger, T., Greiner, E., Stewart, A.F., and Schutz, G. (2001). A CamKIIalpha iCre BAC allows brain-specific gene inactivation. Genesis *31*, 37-42.

Flourakis, M., and Allada, R. (2015). Patch-clamp electrophysiology in Drosophila circadian pacemaker neurons. Methods in enzymology *552*, 23-44.

Gu, H., and O'Dowd, D.K. (2007). Whole cell recordings from brain of adult Drosophila. Journal of visualized experiments : JoVE, 248.

Harrisingh, M.C., Wu, Y., Lnenicka, G.A., and Nitabach, M.N. (2007). Intracellular Ca2+ regulates free-running circadian clock oscillation in vivo. J Neurosci *27*, 12489-12499.

Kula-Eversole, E., Nagoshi, E., Shang, Y., Rodriguez, J., Allada, R., and Rosbash, M. (2010). Surprising gene expression patterns within and between PDF-containing circadian neurons in Drosophila. Proceedings of the National Academy of Sciences of the United States of America *107*, 13497-13502.

Lear, B.C., Darrah, E.J., Aldrich, B.T., Gebre, S., Scott, R.L., Nash, H.A., and Allada, R. (2013). UNC79 and UNC80, putative auxiliary subunits of the NARROW ABDOMEN ion channel, are indispensable for robust circadian locomotor rhythms in Drosophila. PLoS One *8*, e78147.

Lear, B.C., Lin, J.M., Keath, J.R., McGill, J.J., Raman, I.M., and Allada, R. (2005). The ion channel narrow abdomen is critical for neural output of the Drosophila circadian pacemaker. Neuron *48*, 965-976.

Nagoshi, E., Sugino, K., Kula, E., Okazaki, E., Tachibana, T., Nelson, S., and Rosbash, M. (2010). Dissecting differential gene expression within the circadian neuronal circuit of Drosophila. Nature neuroscience *13*, 60-68.

Nash, H.A., Scott, R.L., Lear, B.C., and Allada, R. (2002). An unusual cation channel mediates photic control of locomotion in Drosophila. Curr Biol *12*, 2152-2158.

Pfeiffenberger, C., Lear, B.C., Keegan, K.P., and Allada, R. (2010). Processing sleep data created with the Drosophila Activity Monitoring (DAM) System. Cold Spring Harbor protocols *2010*, pdb prot5520.

Seluzicki, A., Flourakis, M., Kula-Eversole, E., Zhang, L., Kilman, V., and Allada, R. (2014). Dual PDF signaling pathways reset clocks via TIMELESS and acutely excite target neurons to control circadian behavior. PLoS Biol *12*, e1001810.